

Interpretable machine learning-driven optimization of physicochemical properties in hydrogel scaffolds to promote macrophage polarization

Zhaopu Han^{1,2,3#}, Yangguang Huang^{4#}, Zhibao Chen^{1,2,3#}, Tingting Tan⁵, Yucai Li^{1,2,3}, Yujie Chen^{1,2,3}, Linfeng Xu^{1,2,3}, Pengfei Xia^{1,2,3*}, and Xiaojian Ye^{1,2,3*}

ABSTRACT

The physicochemical properties of hydrogel scaffolds, including storage modulus, loss modulus, swelling ratio, porosity, pore size, and roughness, are capable of promoting macrophage polarization into anti-inflammatory phenotype (M2) to accelerate tissue repair. However, most current studies focus on the effects of individual properties on M2 polarization, examining each in isolation. Enhancing the synergistic effects of multiple physicochemical properties is a challenge. In this work, a novel strategy called interpretable machine learning-driven optimization of physicochemical properties (IML-OPP) is proposed to address this challenge. In the IML-OPP strategy, the optimal value of each physicochemical property was sequentially determined based on its ranked importance. First, an initial value was identified for each property by maximizing the individual effect to promote M2 polarization. Then, these initial values were optimized based on their interactive effects. Once all the optimal values were determined, an optimized combination of physicochemical properties was designed to construct a hydrogel scaffold optimized for promoting M2 polarization. To assess the robustness and universality of the IML-OPP strategy, three optimized combinations of physicochemical properties were generated and evaluated. These results offer theoretical guidance for designing hydrogel scaffolds aimed at promoting M2 polarization.

Keywords:

Hydrogel scaffolds; Machine learning; Macrophage polarization; Physicochemical properties

#Authors contributed equally.

*Corresponding authors:

Pengfei Xia,
xiapengfei@shsmu.edu.cn;
Xiaojian Ye,
yxj4380@sjtu.edu.cn.

How to cite this article:

Han Z, Huang Y, Chen Z, et al. Interpretable machine learning-driven optimization of physicochemical properties in hydrogel scaffolds to promote macrophage polarization. *Biomater Transl.* 2025

doi: [10.12336/bmt.24.00088](https://doi.org/10.12336/bmt.24.00088)



1. Introduction

Macrophages are immune effector cells derived from monocytes and play important roles in a variety of physiological processes. They can participate throughout the tissue repair process due to their ability to polarize into either classically activated macrophages (M1) or alternatively activated macrophages (M2) under different inducing conditions.¹ In the early stages of injury, macrophages stimulated by the inflammatory environment polarize into the M1 phenotype and secrete proinflammatory cytokines, such as tumor necrosis factor- α (TNF- α), interleukin (IL)-6, IL-12, and IL-1 β , which exacerbate the inflammatory response and participate in the host defense against pathogen

infection. Later in this microenvironment, macrophages tend to transform into M2 phenotype under the influence of activated Type II cytokines, including IL-4 and IL-13. By secreting anti-inflammatory cytokines, such as IL-4, IL-10, vascular endothelial growth factor, and transforming growth factor- β (TGF- β), M2 polarization modulates the inflammatory environment, promoting the angiogenesis and formation of collagen.^{2,3}

Design strategies for hydrogel scaffolds aimed at promoting M2 polarization are becoming popular in tissue engineering for treating diseases across different systems. At present, the most frequent strategy is loading IL inducers or immunologically active molecules into

ML-guided hydrogel design for M2 polarization

hydrogel scaffolds to regulate M2 polarization.^{4,5} However, challenges such as poor controlled release ability, difficulties in determining optimal dose and frequency, and potential drug resistance limit its application. Therefore, it is necessary to explore new strategies to enhance M2 polarization efficiency in hydrogel scaffolds.^{4,6}

At present, it has been reported that certain physicochemical properties of hydrogel scaffolds are capable of guiding M2 polarization.^{7,8} Among them, the storage modulus (G') and loss modulus (G''), which can activate the reactive oxygen species-mediated nuclear factor kappa B (NF- κ B) signaling pathway, have been shown to positively influence M2 polarization with increasing values of G' and G'' .^{9,10} The pore size (PS) and porosity (P), which are associated with the transcription factors peroxisome proliferator-activated receptor gamma, signal transducer and activator of transcription 6 (STAT6), NF- κ B, and STAT1, have been reported to promote M2 polarization.^{11,12} The swelling ratio (SR), a reflection of hydrophilicity, has been proven to induce M2 polarization through the phosphoinositide 3-kinase and NF- κ B pathways.^{13,14} The roughness (R), an index measuring the surficial topology of hydrogel scaffolds, is believed to stimulate M2 polarization through the Wnt pathway.¹⁵ The regulatory effects of these properties demonstrate that M2 polarization can be regulated by the physicochemical properties of hydrogel scaffolds. However, current studies predominantly focus on the effect of individual properties on M2 polarization. In contrast, multiple physicochemical properties inherently coexist and interact within hydrogel scaffolds. Their synergistic effects could significantly facilitate M2 polarization. To date, few studies have investigated the synergistic effects of multiple physicochemical properties. Theoretically, conducting a large number of one-factor orthogonal experiments could optimize the synergistic effects of multiple physicochemical properties to promote M2 polarization. However, the one-factor orthogonal method is time-consuming and inefficient, making it impractical in real-world applications.¹⁶

In recent years, with the deep integration of information technology and biomedicine, some biomedical issues are expected to be efficiently addressed using information technology.¹⁷ Interpretable machine learning (IML) is an information technology modeling method that can explain quantitative relationships between different factors based on existing data, showing significant advances in accuracy and efficiency. Using IML, predictions can be directly made by inputting specific feature data.¹⁸ In medical research, IML has been widely applied to regulate biological processes.¹⁹ For example, IML has shed light on how various risk factors impact the occurrence and progression of different types of tumors, thereby providing some risk thresholds for tumor prevention.^{20,21} In addition, IML has been used to enhance cell

behaviors when cultured with scaffolds constituted of multiple bioactive materials. By aiming at maximizing cell growth, viability, or antibacterial properties, the optimal material composition can be determined.^{22,23} As demonstrated, current medical applications highlight the potential of IML, which is highly promising for understanding how to enhance the synergistic effects of multiple physicochemical properties on M2 polarization in hydrogel scaffolds.

In this study, a novel strategy called IML-driven optimization of physicochemical properties (IML-OPP) is proposed for designing hydrogel scaffolds by enhancing the synergistic effects of physicochemical properties on M2 polarization. To develop the strategy, data on physicochemical properties and M2 polarization are collected from high-quality literature. After feature selection and data normalization, a dataset consisting of seven features and 60 samples is compiled. Based on this dataset, 21 different types of IML models are trained with hyperparameter optimization. Subsequently, eight metrics and confusion matrices are individually used to compare the performance of these models. The best IML model is then selected to interpret the importance ranking, as well as the independent and interactive effects of physicochemical properties on M2 polarization. Finally, three optimized combinations of physicochemical properties are generated to verify the robustness and universality of the IML-OPP strategy. A schematic illustration of how the IML-OPP strategy is constructed and applied in this work is shown in **Figure 1**. Overall, the IML-OPP strategy is expected to facilitate M2 polarization through the regulation of the physicochemical properties of hydrogel scaffolds.

2. Methods

2.1. Dataset construction

2.1.1. Data mining

Literature was retrieved using “macrophage,” “hydrogel scaffold,” and “polarization” as keywords in the Scopus database (<https://www.scopus.com/>). The subject areas were limited to “Engineering, Multidisciplinary, Biochemistry, Genetics and Molecular Biology, Materials Science, Medicine, and Chemical Engineering,” and the document type was limited to “Article,” with the publication period limited to 2014 – 2024. To gather more high-quality literature, additional searches were conducted in the PubMed database (<https://pubmed.ncbi.nlm.nih.gov/?myncbshare=pubmedplus>), CNKI database (<https://www.cnki.net>), and Google Scholar database (<https://scholar.google.cz/schhp?hl=zh-CN>) using the same retrieving strategy.

Among all the relevant literature, samples with the potential to be included in the IML dataset were selected according to the following criteria. To ensure diversity and representativeness in the dataset, it was necessary to maintain a relative balance of samples with different material compositions and synthesis

¹Department of Orthopedics, Tongren Hospital, Shanghai Jiao Tong University School of Medicine, Shanghai, China; ²Center for Spinal Minimally Invasive Research, Shanghai Jiao Tong University, Shanghai, China; ³Shanghai Key Laboratory of Flexible Medical Robotics, Tongren Hospital, Institute of Medical Robotics, Shanghai Jiao Tong University, Shanghai, China; ⁴Department of Pharmacy, Tongren Hospital, Shanghai Jiao Tong University School of Medicine, Shanghai, China; ⁵Department of Critical Care Medicine, Shanghai Tenth People's Hospital, Tongji University School of Medicine, Shanghai, China

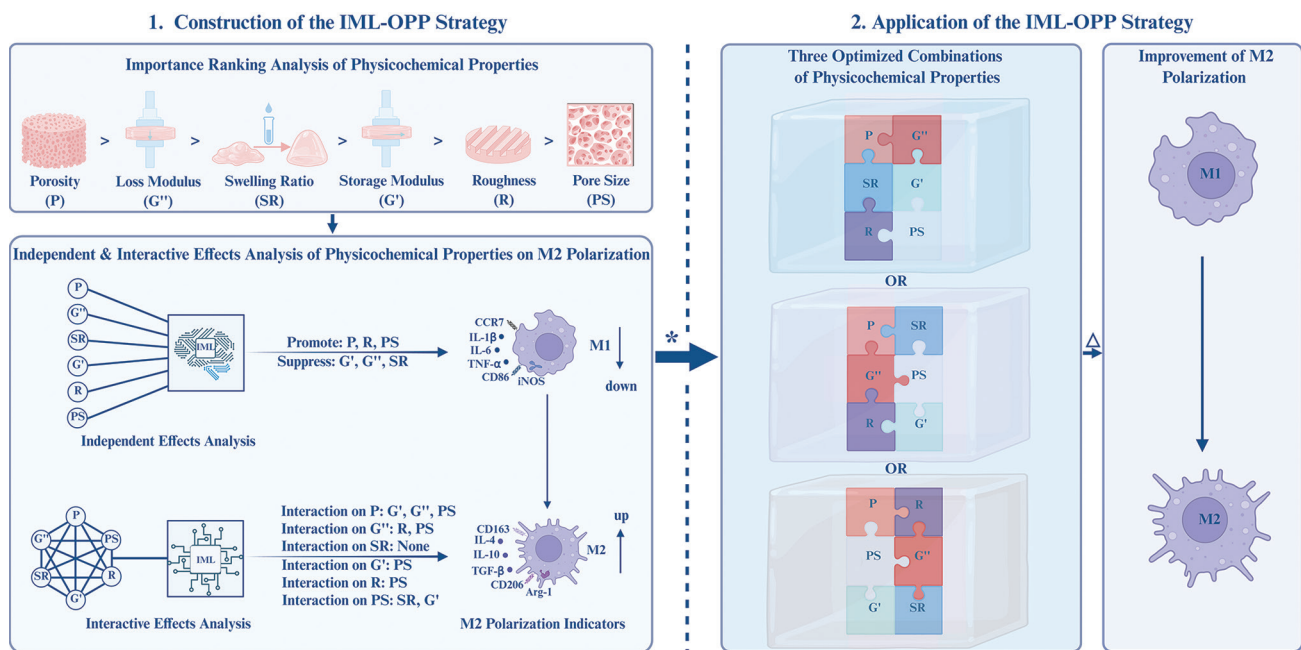


Figure 1. Schematic illustration of the construction and application of the IML-OPP strategy. Created with BioRender.com. Han, Z. (2025) <https://BioRender.com/pwureur>. Notes: *: Improve the synergistic effects of multiple physicochemical properties; Δ : Promote M2 polarization to the highest possible level using hydrogel scaffolds.

Abbreviations: Arg-1: Arginase-1; CCR7: C-C chemokine receptor type 7; CD86: Cluster of differentiation 86; CD163: Cluster of differentiation 163; CD206: Cluster of differentiation 206; G': Storage modulus; G'': Loss modulus; IL-1 β : Interleukin-1 beta; IL-4: Interleukin-4; IL-6: Interleukin-6; IL-10: Interleukin-10; iNOS: Inducible nitric oxide synthase; P: Porosity; PS: Pore size; R: Roughness; SR: Swelling ratio; TGF- β : Transforming growth factor beta; TNF- α : Tumor necrosis factor alpha; IML-OPP: Interpretable machine learning-driven optimization of physicochemical properties.

processes. For example, the methods most widely used for preparing hydrogels in recent years were prioritized by including a larger number of samples related to those scaffolds. Similarly, hydrogel scaffolds synthesized from widely used raw materials were considered during data augmentation. Regarding the scaffold form, it was necessary to ensure that all hydrogel scaffolds included in the dataset were traditional bulk scaffolds, excluding newer types such as hydrogel microspheres and microneedles. This approach aimed to reduce the potential impact of different scaffold forms on the effects exerted by various physicochemical properties, thereby controlling the confounding bias during model training.

From the perspective of cell culture, first, the selected samples must reflect the incubation processes of macrophages on the surface of hydrogel scaffolds with varying physicochemical properties. This excluded samples where macrophages were cultured in the extracts or base solutions of hydrogel scaffolds, especially those samples adopting the Transwell technique. This criterion was set to maximize the effects of physicochemical properties on M2 polarization through direct contact between macrophages and the hydrogel scaffolds. Moreover, it could harmonize cultivation methods across studies to eliminate the interference of differing practices on the results.

Second, to minimize the influence of non-physicochemical factors on M2 polarization and enhance the credibility of the dataset, the included hydrogel scaffolds should not contain active ingredients that promote M2 polarization, such as cytokines (e.g., TGF- β and IL-4) and metal ions (e.g., Mg²⁺ and Zn²⁺).

Third, to minimize between-group differences and enhance the homogeneity of outcome indicators, the cell line applied in the selected samples should be unified. The Raw264.7 cell line, a widely used model for *in vitro* culture of macrophages, was considered an ideal candidate.

Fourth, to balance the effects of different polarization conditions across studies and ensure comparability of outcome indicators, the experiments corresponding to the selected samples must include positive controls.

Finally, to confirm the metrizable of the outcome indicators, M2 polarization must be evaluated using at least one of the following techniques: western blotting (WB), flow cytometry (FC), enzyme-linked immunosorbent assay (ELISA), or quantitative polymerase chain reaction (qPCR).

2.1.2. Data preprocessing

In terms of feature selection, to ensure the representativeness of the properties during the incubation process with macrophages and considering their prevalence in the literature, four categories of hydrogel scaffold properties were initially extracted, including mechanical properties, hydrophilicity, pore properties, and surface morphology. These four categories encompassed multiple initial features reflecting different aspects of physicochemical properties. To reduce the overfitting risk caused by the imbalance between the number of samples and features, the maximal information coefficient (MIC) was used to measure the correlation between the extracted original features and the outcome indicators.²⁴ After ranking the MICs of all initial features, a threshold was set,

ML-guided hydrogel design for M2 polarization

rejecting any features with an MIC lower than 0.1. Eventually, six physicochemical properties were selected as the included features: G' , G'' , SR, R, P, and PS.

To ensure consistent measuring standards for these properties across all samples, G' and G'' were collected uniformly at a strain of 0.5 – 1% and a frequency of 1 Hz. For SR, the time point at which a submerged hydrogel scaffold reached an equilibrium swelling state in 1×phosphate-buffered saline (pH 7.4) at room temperature was selected as the endpoint. The SR was calculated by determining the difference between the wet weight at the endpoint and the dry weight before submerging the hydrogel scaffold and then dividing this difference by the dry weight. For R, P, and PS, they were acquired by analyzing data from a scanning electron microscope (SEM) using ImageJ software. Specifically, PS represented the average projected area of multiple pores on the surface of the hydrogel scaffolds, while P indicated the average proportion of the porous area on the surfaces of hydrogel scaffolds. Notably, R was defined in a novel way as the coefficient of variation calculated from the gray distribution of a representative area on the hydrogel scaffold surface in the SEM field. This approach was proposed due to the limited studies that precisely quantified the R of hydrogel scaffolds.

To comprehensively evaluate the degree of M2 polarization, a classification index was constructed by combining changes in surface antigens, specific intracellular proteins, and secreted cytokines throughout the M2 polarization process. Specifically, the polarization-related metrics for each sample in the dataset were classified into two types after extraction. The first type was related to proinflammatory indicators, including C-C chemokine receptor type 7, cluster of differentiation 86 (CD86), inducible nitric oxide synthase, TNF- α , IL-1 β , and IL-6. An increase in the levels of these indicators indicated a reduction in M2 polarization. The second type was related to anti-inflammatory indicators, including CD206, CD163, arginase-1, TGF- β , IL-4, and IL-10. An increase in their expression levels indicated an increase in M2 polarization. Scores were then assigned based on the M2 polarization evaluation techniques used in each study, with different criteria applied accordingly.

Briefly, when the study of a sample evaluated polarization-related metrics using WB, ELISA, or qPCR, scores were assigned based on the ratio of the experimental group's value to the positive control group's value. If this ratio was between 0.8 and 1.25, a contribution of 0 was given. If the ratio was between 0.5 and 0.8, a score of +1 was given for proinflammatory-related indicators, and a score of –1 was assigned for anti-inflammatory-related indicators. If the ratio was between 1.25 and 2, a penalty of –1 was imposed for proinflammatory-related indicators, and a score of +1 was given for anti-inflammatory-related indicators. If the ratio was lower than 0.5, a score of +2 was given for proinflammatory-related indicators, and a score of –2 was assigned for anti-inflammatory-related indicators. If the ratio was higher than 2, a penalty score of –2 was given for pro-inflammatory-related indicators, and a score of +2 was given for anti-inflammatory-related indicators.

Similarly, when the study of a sample used FC to evaluate polarization-related metrics, a contribution of 0 was given if the difference between the experimental group's value and the positive control group's value was between –5% and +5%. If the difference was between –10% and –5%, a score of +1 was given for proinflammatory indicators, and a score of –1 was given for anti-inflammatory indicators. If the difference was below –10%, a score of +2 was assigned for proinflammatory indicators, and a score of –2 was given for anti-inflammatory indicators. If the difference was above +10%, a score of –2 was given for proinflammatory indicators, and a score of +2 was assigned for anti-inflammatory indicators.

Finally, the cumulative score of each sample across all indicators was calculated and then divided by the number of evaluation indicators corresponding to that sample to obtain the average value. If the average value was positive, it was rounded to the nearest whole number according to standard rounding principles. Otherwise, all values were set to 0. Eventually, a target system measuring the degree of M2 polarization on a scale of 0, 1, or 2 was established. In this system, samples with a target value of 0 indicated that macrophages were either not significantly polarized to M2 or even polarized toward M1 under the given combinations of physicochemical properties. Likewise, samples with a target 1 indicated slight M2 polarization in macrophages cultured on these hydrogel scaffolds. Samples with a target value of 2 indicated significant M2 polarization of macrophages.

After data reduction and normalization, a dataset with seven features and 60 samples was compiled for IML (**Table S1**). Each column, except for the last, represented a specific feature, with all values in each column having the same unit. The last column of the dataset represented the outcome target, which indicated the synergistic effects of hydrogel scaffolds on M2 polarization under specific combinations of physicochemical properties. Notably, data augmentation was performed to include additional samples. This technique helped to prevent underfitting or overfitting, which could occur with a small training set and unbalanced classes.

2.2. IML model training and evaluation

2.2.1. Hyperparameter optimization

A total of 21 IML models were included in this study for performing a multi-classification task. These models are widely recognized ML models in the biomedical field for their reliability in terms of model complexity, popularity, scalability, and interpretability.^{23,25,26} The most appropriate model was identified through an exhaustive comparison utilizing various evaluation metrics. Specifically, to reduce the risk of overfitting while enhancing the robustness of each model, a five-fold cross-validation approach was employed, where the dataset was randomly divided into training and testing subsets with an 80:20 ratio. For hyperparameter optimization to determine the optimal combinations, grid search, a reliable method, was employed to systematically screen the representative hyperparameters, tailored to each model's unique characteristics.²³ **Table 1** provides a concise summary of the definitions and characteristics of each IML model presented in

this study, along with the optimized hyperparameters based on packages such as scikit-learn and PyTorch.

2.2.2. Optimal model selection

In accordance with the methodology proposed by Rafieyan *et al.*,²³ the current study selected seven metrics to assess the predictive capabilities of the models from various perspectives. These metrics included accuracy, precision, recall, F1 Score, Cohen's kappa coefficient (CKC), Matthews correlation coefficient (MCC), and the area under the receiver operating characteristic curve (ROC_AUC).²⁷

Accuracy is the proportion of correctly predicted samples to the total number of predictions in classification models. As a comprehensive metric, accuracy is the most prevalently used in IML studies. However, it is susceptible to invalidation in the event of sample imbalance. Precision refers to the frequency with which the model correctly predicts the positive class, while recall refers to the proportion of correctly identified positive class labels out of all possible positive class labels. As two metrics evaluating the reliability of positive predictions from distinct viewpoints, precision, and recall often cannot attain their maximum values concurrently. The F1 Score, being the harmonic mean of these two, provides a stable assessment while maintaining a balance between them. CKC is commonly employed to quantify the degree of consistency between two evaluation systems. It ranges from -1 to 1 , with the significant advantage of rectifying accidental consistency in the classification process. MCC, another integrated classification metric ranging from -1 to 1 , balances the influence of true positives, true negatives, false positives, and false negatives. It is particularly suitable for situations with small sample sizes and unbalanced classes. The ROC_AUC represents a comprehensive evaluation of the prediction effect across all possible classification thresholds. ROC_AUC quantifies the ability to more confidently identify a randomly chosen positive sample as truly positive, compared to the probability of misclassifying a negative sample as positive. This metric is often regarded as the most credible evaluation criterion.

Based on the computation of the seven metrics for each model, a comprehensive score was obtained by summing them. By comparing these scores across the 21 IML models, the optimal IML model for predicting cell behavior on hydrogel scaffolds was identified. In addition, the prediction performance of this optimal model across all classes was visually presented using a confusion matrix.

2.3. Importance ranking analysis

Most IML models, which primarily focus on training and prediction, are considered "black-box models" and have limited interpretability. Therefore, it is necessary to deconstruct these models after their establishment to understand how variations in each feature contribute to the changes in targets. The Shapley additive explanations (SHAP) algorithm offers a comprehensive approach to IML model interpretation. Its fundamental principle involves constructing an additive explanatory model by calculating the marginal contribution of each feature to the predicted targets after model prediction.

This allows for an in-depth understanding of the direction and magnitude of each feature's influence at both global and individual levels.²⁸

For different IML models, the SHAP algorithm can be matched with various explanatory tools, such as gradient, linear, tree, and kernel explainers, to provide accurate interpretations of specific IML models. After determining explainers, the importance ranking of all features can be computed and visualized at both individual and global levels. Ideally, these rankings should be consistent across both levels, reflecting the robustness of the analyzed IML model. However, in practice, importance rankings often vary between individual samples and the global-level interpretation is considered more reliable in these cases. In the current study, the importance ranking of six physicochemical properties in promoting M2 polarization was determined using the optimal IML model. This ranking guided the optimized order of physicochemical properties in the IML-OPP strategy.

2.4. Independent effect analysis

The independent effects of each physicochemical property were analyzed using scatter plots, depicting how the SHAP values varied with changes in property values for each sample in the testing set. The tendency of increment or decrement of data points across different property values reflected the direction of independent effects, both at the local and global levels. These trends served as important elements for optimizing physicochemical properties in the IML-OPP strategy.

2.5. Interactive effect analysis

The interactive effects of each physicochemical property with other properties were analyzed using dependence plots, which illustrated how the SHAP value of a given property varied when that property was held constant while others changed. The trends – whether increasing or decreasing – of data points under relatively fixed property values reflected the directions of interactive effects across different value ranges. These trends were considered another critical factor for optimizing physicochemical properties in the IML-OPP strategy.

2.6. Analysis tools

This study used the AutoDL platform (SeetaCloud Nanjing Technology, China), Python software (version 3.12, Python Software Foundation, USA), ImageJ 1.54d software (National Institutes of Health, USA), GraphPad Prism 8 software (GraphPad Software, USA), Biorender APP (Biorender, Canada), and WPS software (version 12.1.0.16729, Kingsoft Office Software, China) for data summarization and analysis. The primary Python packages used included NumPy 1.26.3, Matplotlib 3.6.3, scikit-learn 1.4.1.post1, pandas 2.2.0, PyTorch 2.2.0, and shap 0.42.0.

3. Results

3.1. Dataset description

To ensure the applicability of IML models from the perspective of included data and to gain an initial understanding of the significance of each physicochemical property in hydrogel scaffolds, it is crucial to provide an overview of the prevalent

ML-guided hydrogel design for M2 polarization

ranges of these properties. Therefore, before the training and predicting processes of IML models, a descriptive statistical analysis was conducted on the preprocessed dataset. This dataset comprised six physicochemical features – G' , G'' , SR, R, P, and PS. An additional feature, incubation time (IT), reflecting cell co-culture duration, was also included. The target variable included three classes, labeled 0, 1, and 2, representing the degree of M2 polarization in ascending order. The arrangement of multiple features and classified targets facilitated IML model training on the dataset in universal prediction and evaluation, thereby demonstrating the robustness of the dataset.

Figure 2A-F demonstrates the distribution of kernel density estimation of the six physicochemical properties included in

the dataset, both across full target classes and target 2 samples, which exhibited the highest degree of M2 polarization. These distributions, to some extent, reflect the value ranges of each physicochemical property to stimulate macrophage polarization.

For G' (Figure 2A), the maximum probability density was observed around 1,000 Pa in both the full target and target 2 classes, indicating that hydrogel scaffolds prepared for macrophage polarization tended to exhibit low energy G' . In addition, no target 2 samples had G' exceeding 7,000 Pa, suggesting that an excessively high G' may be unfavorable for promoting M2 polarization.

For G'' (Figure 2B), the maximum probability density was observed around 200 Pa in both the full target and target

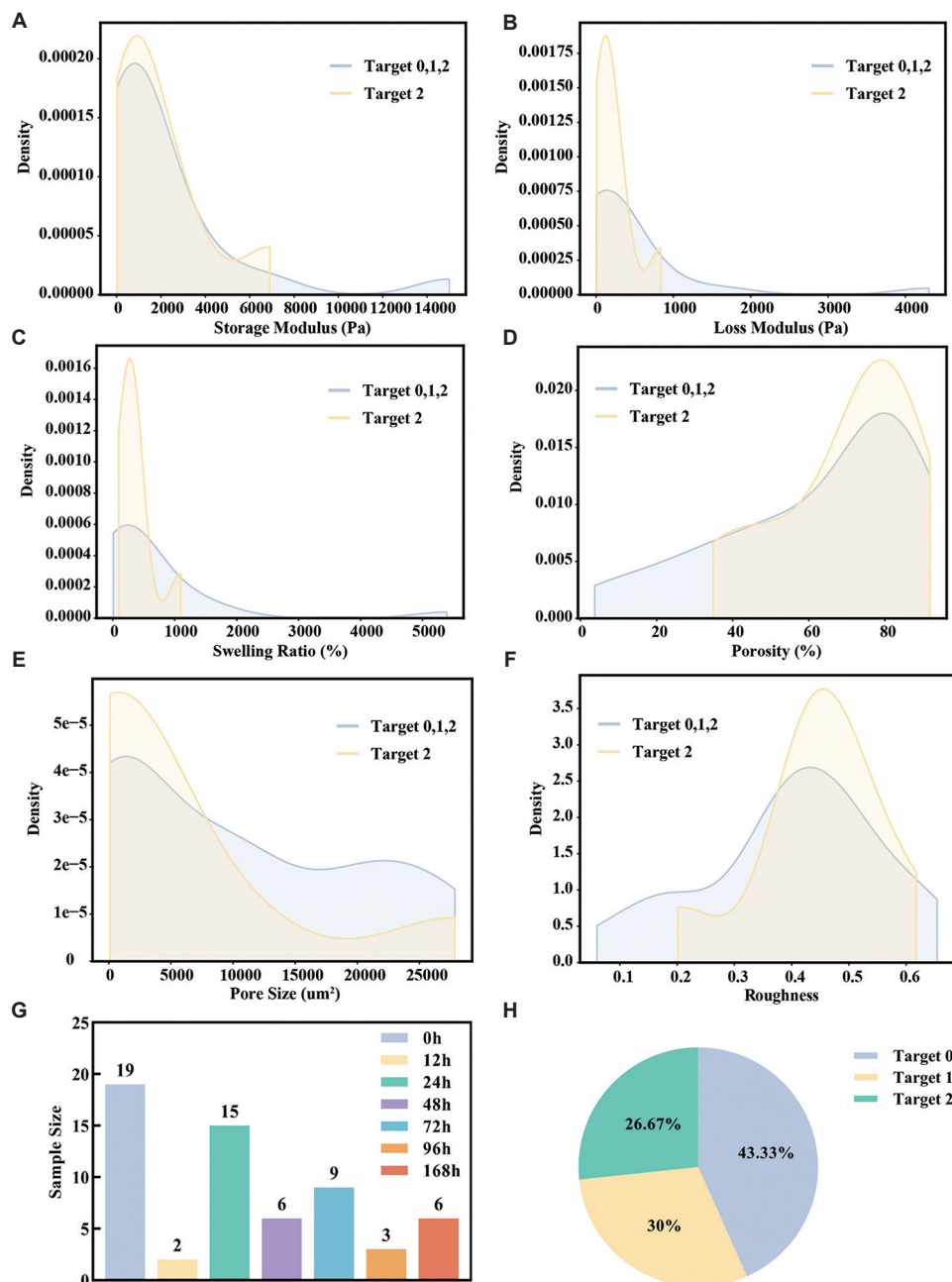


Figure 2. Descriptive statistical analysis for the dataset used in this study. (A-F) Kernel density estimation distribution of storage modulus (G'), loss modulus (G''), swelling ratio (SR), porosity (P), pore size (PS), and roughness (R) on full target and target 2 classes. (G) Frequency distribution of feature incubation time. (H) Balanced distribution of target across three classes.

2 classes, indicating that hydrogel scaffolds prepared for macrophage polarization tended to exhibit low energy G . Besides, no target 2 samples had G exceeding 850 Pa, suggesting that an excessively high G may also be unfavorable for promoting M2 polarization.

For SR (Figure 2C), the maximum probability density was observed to be around 300% in both the full target and target 2 classes, indicating that most hydrogel scaffolds prepared for macrophage polarization had low SR. Additionally, no target 2 samples had SR exceeding 1100% or below 90%, suggesting that excessively high or low SR may hinder M2 polarization.

For P (Figure 2D), the maximum probability density was observed to be around 80% in both the full target and target 2 classes, indicating that hydrogel scaffolds prepared for macrophage polarization tended to have high P. Moreover, no target 2 samples had P below 30%, suggesting that an excessively small P could negatively affect M2 polarization.

For PS (Figure 2E), the maximum probability density was observed around 1,200 μm^2 in both the full and target 2 classes, indicating that most hydrogel scaffolds prepared for macrophage polarization had small PS. Furthermore, the PS distribution range of target 2 samples in the dataset aligned with that of all type samples, indicating that PS may have a weak impact on M2 polarization.

For R (Figure 2F), the maximum probability density was observed around 0.4 – 0.5 for both the full target and target 2 classes, indicating that hydrogel scaffolds prepared for macrophage polarization tended to have moderate R. Moreover, no target 2 samples in the dataset had R below 0.2, suggesting that excessively small R may hinder M2 polarization.

The IT feature and the distribution of the target also highlighted trends observed in current research. Figure 2G illustrates the IT of macrophages cultured with hydrogel scaffolds in the studies corresponding to each sample in the dataset. It is evident that, apart from the 0 h time point, which holds little relevance for discussion, the 24 h time point was most commonly used as the evaluation node for M2 polarization levels. The maximum value of IT in all included samples was 168 h, indicating that the M2 polarization effect of hydrogel scaffolds likely required a longer duration to manifest. Figure 2H shows the proportion of targets 0, 1, and 2 within the dataset, indicating a balanced distribution of target classes. This balance helps mitigate the risk of bias in the target distribution.

3.2. IML model training and evaluation

3.2.1. Hyperparameter optimization

Hyperparameter optimization is an inevitable step in optimal model selection, as it maximizes the performance of each of the 21 IML models on the dataset. By repeatedly training and predicting with different hyperparameter combinations, the optimal combination for each IML model can be identified. Table 2 presents the outcomes of hyperparameter optimization for the 21 IML models.

Among tree-structured models, including the extreme gradient boosting (XGBoost), categorical boosting (CatBoost), light gradient boosting machine (LGBM) Classifier, decision tree

(DT), random forest (RF), extremely randomized trees, and regularized greedy forest (RGF) Classifier, the hyperparameter “n_estimators” or “iterations,” which represents the number of sub-trees, had a significant impact on model performance. Increasing this value enhanced model complexity and improved prediction robustness, but it also raised the risk of overfitting. Meanwhile, the hyperparameter “depth” or “max_depth,” which represents the tree depth, restricted the maximum number of layers during model training. Excessively increasing this value may lead to models capturing extra noise in the training set, increasing the risk of overfitting. The hyperparameter “learning_rate” generally showed an inverse correlation with the aforementioned two types of hyperparameters. A lower learning rate was associated with a more robust model. In addition, the parameters “min_samples_leaf” and “min_samples_split” were used to restrict the branching in tree structures. Higher values of these hyperparameters indicated lower model complexity, which may increase the resistance to model training. For the dataset in this study, most tree-structured models optimized their hyperparameters with moderate values of “n_estimators”/“iterations,” “depth”/“max_depth,” and “learning_rate,” while using relatively low values for “min_samples_leaf” and “min_samples_split.” This setup reflects a balance between increasing model complexity and reducing the risk of overfitting, especially when processing datasets with a small sample size. In particular, to enhance the model’s generalization ability and to accelerate model training, the LGBM Classifier set the hyperparameters “colsample_bytree” and “subsample” to values <1, while the RGF Classifier set the hyperparameter “algorithm” to “RGF” to enhance prediction robustness through a single-leaf model with RGF and L2 regularization.

For neural network (NN)-related models, the NN model represents a classical NN that is learned based on the PyTorch frame. The MLP Classifier, on the other hand, is a relatively simplified version of a fully connected feed-forward NN compared to the NN model. In the current study, both models were trained with the Rectified Linear Unit activation function and Adam adaptive algorithm. However, there was a key difference in the structure of the hidden layers: the NN model was optimized with 64 hidden layers, while the MLP Classifier had only 2 layers. Given the characteristics of the dataset applied in this study, it can be speculated that the NN model may be too complex to perform effectively in prediction.

In the case of the three basic linear models – Logistic Regression, Ridge Classifier, and Passive Aggressive Classifier – as well as the two support vector machine (SVM) classifiers, the SVM and Linear SVC models, regularization plays a crucial role in reducing the risk of overfitting and enhancing the models’ generalization ability. In this study, the regularization hyperparameter “C” for the Logistic Regression and SVM models, as well as the regularization hyperparameter “alpha” for the Ridge Classifier, were adjusted to impose a larger penalty term. This adjustment aimed to reduce the risk of overfitting and enhance model robustness.

For the k-nearest neighbor (KNN) model, the samples in the dataset were grouped into distinct clusters, and the “weights” parameter was set to “uniform.” This configuration ensured

ML-guided hydrogel design for M2 polarization

that all nearest-neighbor samples had equal weights, thereby fully utilizing the information from each sample.

For the discriminant analysis models, the model optimization process involved the calculation of feature covariance matrices. The hyperparameter “reg_param” in the quadratic discriminant analysis (QDA) model and the “shrinkage” parameter in the Linear Discriminant Analysis model were used to regularize the covariance matrices, thereby enhancing model performance.

For models based on the Naive Bayes (NB) assumption, hyperparameter optimization for Gaussian NB was straightforward. The hyperparameter “var_smoothing” was set to its default value in the Gaussian NB model to meet the requirement of computational stability. However, for the Bernoulli NB model, additional factors needed to be considered, such as the smoothing factor “alpha,” the binarization feature threshold “binarize,” and “fit_prior” hyperparameters which determine whether to learn the class prior probabilities. These factors could influence the model’s fitting degree during model training.

During the optimization process of the Gaussian process classifier (GPC) and label propagation models, selecting the hyperparameter “kernel” was crucial. The GPC model was endowed with the general RBF kernel. It could handle samples where the features are non-linearly related to the class targets and reduce the risk of numerical difficulties. Unlike the GPC model, the Label Propagation model performed better with the KNN kernel, likely due to the balanced structure of the dataset.

Overall, the optimized hyperparameters for the 21 IML models were presented, facilitating further evaluation and comparison of the performances of IML models.

3.2.2. Optimal IML model selection

After hyperparameter optimization, the 21 IML models were expected to demonstrate excellent performances. However, the key objective was to identify the model with the best predictive ability in establishing the relationship between the physicochemical properties of hydrogel scaffolds and M2 polarization levels. For this purpose, seven evaluation metrics were used to evaluate the prediction performance of the 21 IML models from different perspectives (**Figure 3A-H**).

Overall, among the 21 IML models, the maximum value for accuracy and recall was 0.8333, while the minimum value was 0.2500, and the median was 0.6667. Similarly, for precision, F1 Score, ROC_AUC, CKC, and MCC, the maximum values were 0.8889, 0.8296, 0.9881, 0.7500, and 0.7828, respectively, while the minimum values were 0.1736, 0.2451, 0.5381, -0.1739, and -0.1822, respectively. The medians for metrics distribution were 0.7183, 0.6508, 0.8232, 0.4839, and 0.4892, respectively. These results indicate that, although there were significant performance differences among the 21 IML models, most models exhibited some level of predictive value for the polarization behavior of macrophages cultured on hydrogel scaffolds. This suggests that the dataset is reliable.

Focusing on the optimal models across each metric, six models consistently demonstrated outstanding performance in all metrics: RF, DT, Catboost, QDA, XGBoost, and MLP Classifier. Moreover, when the sum of the seven evaluation metrics was

used to evaluate the performance of each model, these six models emerged as the top performers (**Figure 3H**). Since the goal of applying ML models was to explore the combination of physicochemical properties of hydrogel scaffolds that most effectively promote M2 polarization, it was necessary to compare the predictive abilities of different models for various target classes to identify the model most accurate in predicting target 2 samples. Among these six top-performing IML models, confusion matrices were used to illustrate the combinations of actual and predicted target classes for each model (**Figure 4**). It was obvious that when RF, DT, Catboost, and MLP Classifier models were used to predict the test set, the probability of accurate prediction for samples with actual target 1 or 2 reached 100%, and when predicting target 2 samples, the models perfectly matched the actual target (**Figure 4A, and C-E**). In contrast, the QDA model was only able to achieve 66.7% accuracy for predicting actual target 2 samples, while the XGBoost model showed a relatively high misjudgment rate for predicting target 2 samples (**Figure 4B and F**).

Summarizing the evaluations above, the RF model not only excelled in five metrics – accuracy, precision, recall, CKC, and MCC – but also achieved the highest overall evaluation when considering the sum of all metrics. More importantly, the confusion matrix for the RF model demonstrated the most accurate predictions for samples with target 2, highlighting its potential for promoting M2 polarization. Therefore, the RF model was selected as the best IML model. Detailed parameters are available in the model file “HydrogelScaffoldProperties_MacrophagePolarization_RF.pkl” in the **Supplementary Materials**.

3.3. Importance ranking analysis of the six physicochemical properties

Through hyperparameter optimization and multi-angle performance evaluation, the optimal RF model was established. However, as a black box model, without further processing, it could only be used to predict the degree of M2 polarization promotion induced by hydrogel scaffolds with specific combinations of physicochemical properties. This limitation made it challenging to directly understand how these physicochemical properties synergistically influenced M2 polarization. Therefore, it was necessary to conduct an interpretability analysis of the selected optimal IML model.

The SHAP algorithm, an additive explanation method for ML model interpretability analysis in recent years, was introduced in this study to analyze the optimal RF model. Given that the optimal RF model is characterized by a tree structure, the tree explainer was selected as the core of the SHAP algorithm for analysis.

To determine the importance ranking of different physicochemical properties in hydrogel scaffolds influencing M2 polarization, the effects of each physicochemical property at the individual sample level were first explored. As shown in **Figure 5A-C**, the first three samples in the test set exhibited completely different impact directions and levels among the seven features, indicating that the importance ranking of physicochemical properties reflected by each sample may not be unified. Therefore, we switched to exploring the importance of ranking at the global level. As presented in **Figure 5D**, the

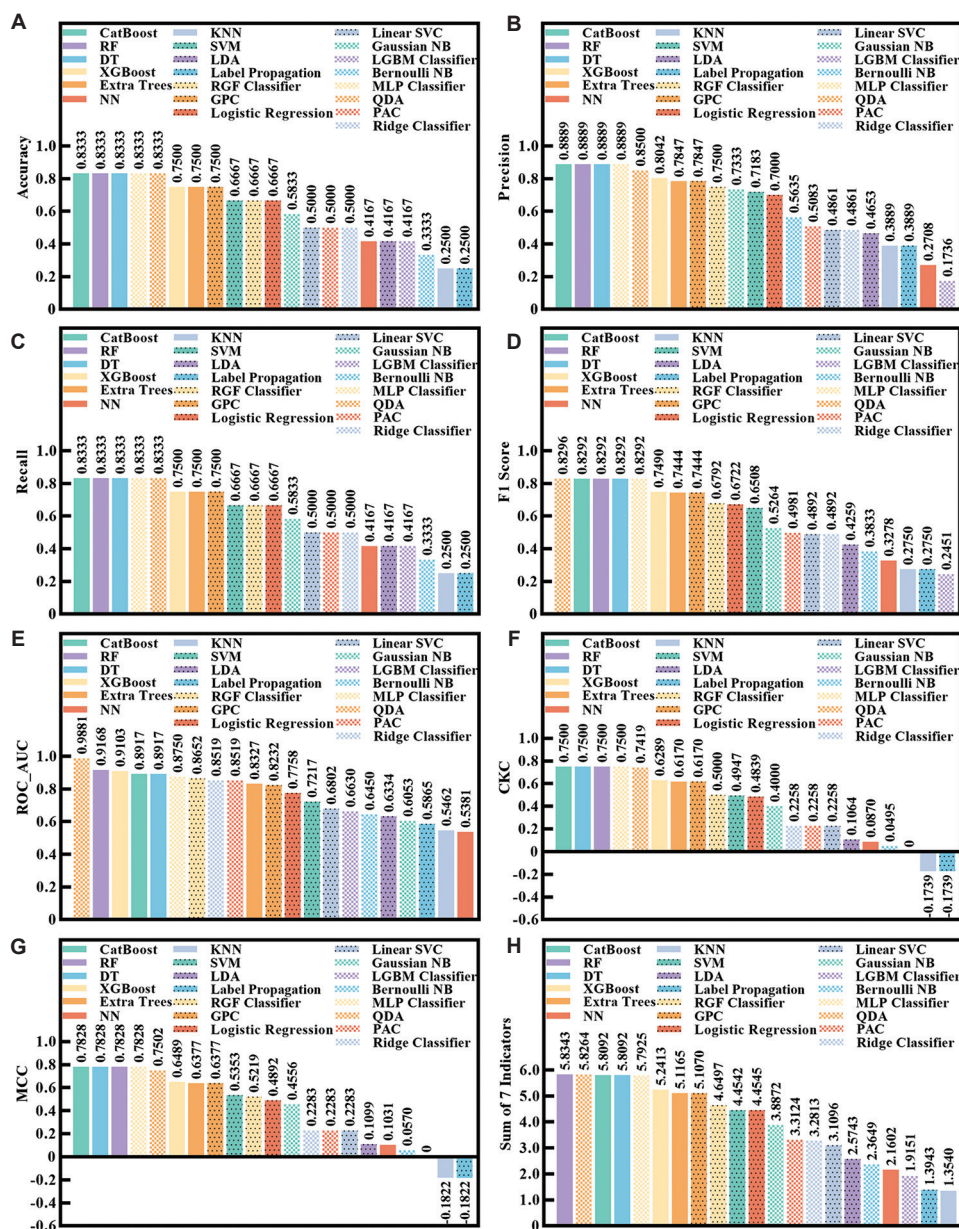


Figure 3. Predictive performances comparison on (A) accuracy, (B) precision, (C) recall, (D) F1 Score, (E) ROC_AUC, (F) CKC, (G) MCC, and (H) the sum of the first seven metrics of 21 interpretable machine learning models.

Abbreviations: Bernoulli NB: Bernoulli Naive Bayes; CatBoost: Categorical boosting; DT: Decision tree; Extra Trees: Extremely randomized trees; Gaussian NB: Gaussian Naive Bayes; GPC: Gaussian process classifier; KNN: K-nearest neighbors; LDA: Linear discriminant analysis; LGBM: Light gradient boosting machine; Linear SVC: Linear support vector classification; MLP: Multi-layer perceptron; NN: Neural network; PAC: Passive aggressive classifier; QDA: Quadratic discriminant analysis; RF: Random forest; RGF: Regularized greedy forest; SVM: Support vector machine; XGBoost: Extreme gradient boosting; ROC_AUC: Area under the receiver operating characteristic curve; CKC: Cohen's kappa coefficient; MCC: Matthews correlation coefficient.

importance ranking of the six physicochemical properties for M2 polarization, in descending order, was P, G^{''}, SR, G', R, and PS. Building on this basis, **Figure 5E** depicts the impact directions of each feature, including that of IT. The results showed that the most important property for M2 polarization at the global level was P. Within the range of 3.764 – 91.824% corresponding to the training set, increasing P will most likely promote M2 polarization. Interestingly, though R and PS ranked lowest in importance, they also showed a positive correlation with M2 polarization at the global level. In contrast, G^{''}, G', and SR were negatively correlated with M2 polarization. In addition, the effect of IT on M2 polarization

was consistent with the expectation, that is, within the range of 0 – 168h corresponding to the training set, suggesting that increasing the IT is conducive to M2 polarization. In summary, these results establish a priority sequence for optimizing physicochemical properties. For example, unless there are fixed demand for its value, P should be prioritized when optimizing a single physicochemical property to promote M2 polarization.

3.4. Independent effect analysis of the six physicochemical properties

To enhance the synergistic effects of multiple physicochemical properties, it is necessary to fully understand the independent

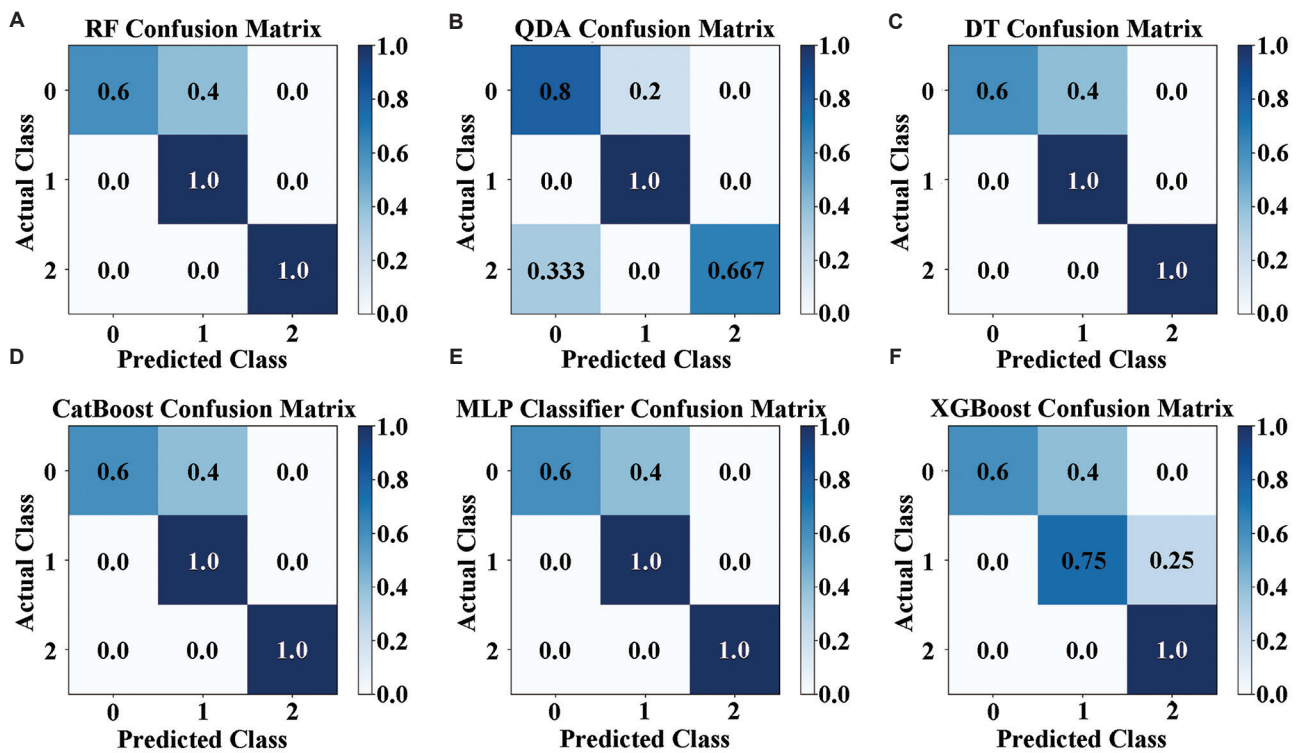


Figure 4. Confusion matrix of interpretable machine learning models of (A) RF, (B) QDA, (C) DT, (D) CatBoost, (E) MLP classifier, and (F) XGBoost.

Abbreviations: RF: Random forest; QDA: Quadratic discriminant analysis; DT: Decision tree; CatBoost: Categorical boosting; MLP: Multi-layer perceptron; XGBoost: Extreme gradient boosting.

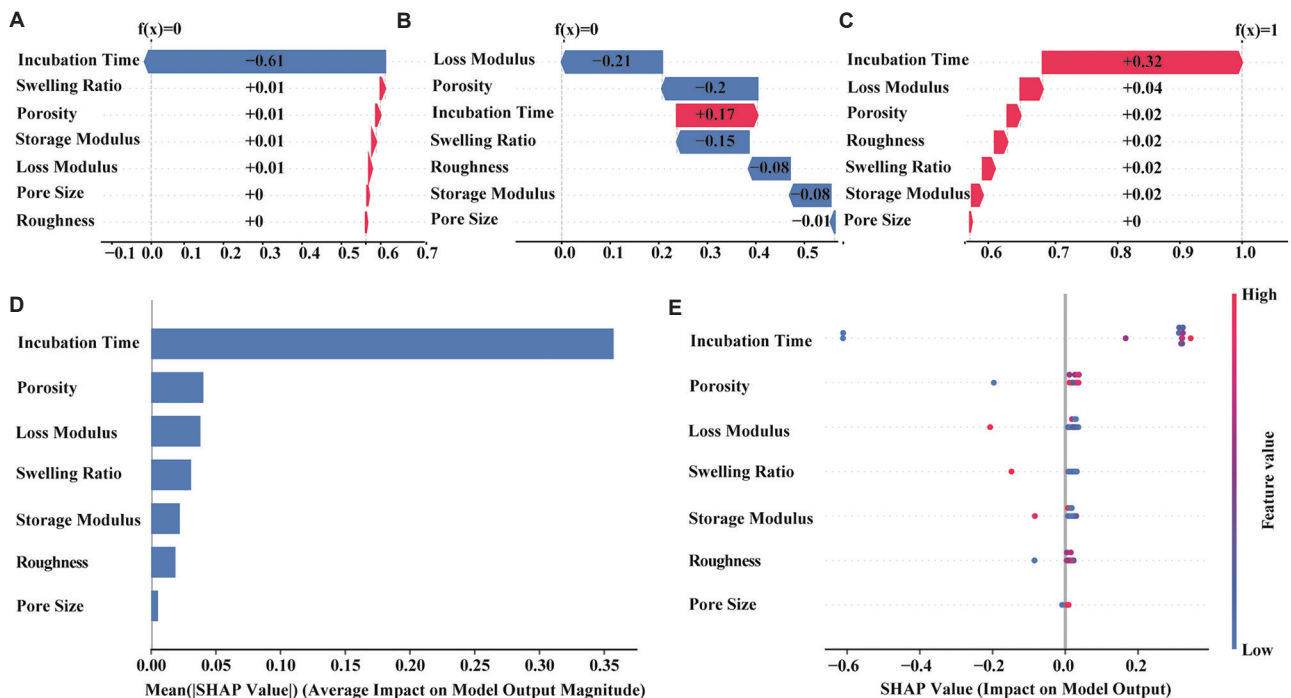


Figure 5. Importance ranking analysis on the optimal random forest model. (A-C) Feature contribution to M2 polarization at individual level for the first three samples in the test set. (D) Importance ranking of feature contribution at the global level. (E) Impact directions and levels of each feature on M2 polarization.

Abbreviation: SHAP: Shapley additive explanations.

effect of each property. To achieve this, scatter plots of the SHAP value distributions for each physicochemical property were generated based on the test set data (Figure 6).

Figure 6A shows that only when the P was between 3.764% and 48.063% did an increase in P markedly promote M2 polarization. Conversely, when P varied between 48.063% and

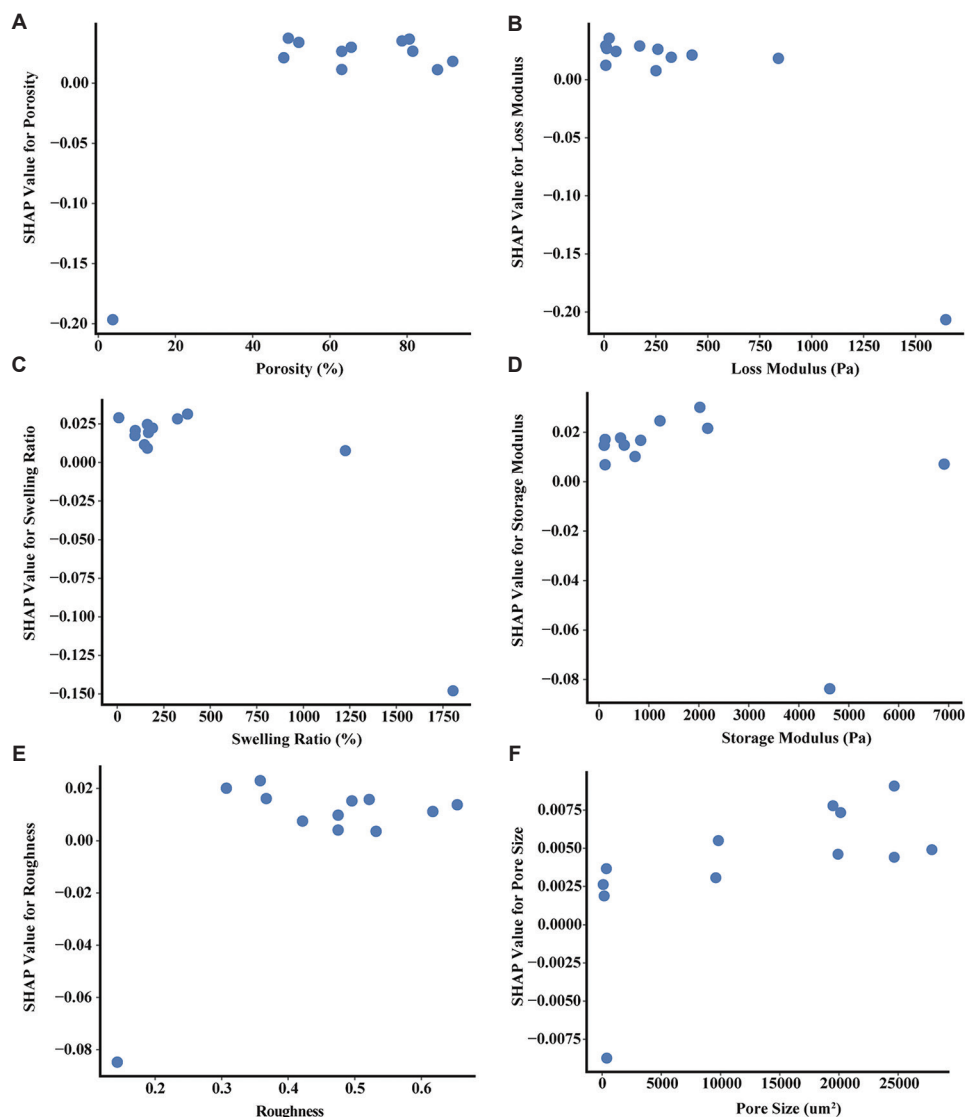


Figure 6. Scatter plots for SHAP values of (A) porosity (P), (B) loss modulus (G''), (C) SR, (D) storage modulus (G'), (E) roughness (R), and (F) PS, reflecting independent effects on M2 polarization of each physicochemical property. Abbreviations: SHAP: Shapley Additive Explanations; SR: Swelling ratio; PS: Pore size.

91.824%, its changes had minimal impact on M2 polarization. These results suggest that in designing hydrogel scaffolds aimed at promoting M2 polarization, it may not be necessary to pursue an excessively high P.

Figure 6B displays that when the G'' was between 839.599 Pa and 1,645.570 Pa, its decrease markedly promoted M2 polarization. In contrast, when the G'' varied between 8.653 Pa and 839.599 Pa, its decrease made a relatively low contribution to M2 polarization. These findings indicate that excessively low G'' may offer limited benefits for hydrogel scaffold optimization.

Figure 6C demonstrates that when the SR was between 377.815% and 1,804.511%, its decrease markedly promoted the polarization of M2. This result is consistent with the effect direction obtained in the section importance ranking analysis of the six physicochemical properties. However, a slight tendency to inhibit M2 polarization was observed as the SR decreased in the range of 8.372% – 377.815%. This suggests

that a moderate SR is beneficial for enhancing the promoting effect of hydrogel scaffolds on M2 polarization.

Figure 6D reveals that when the G' was between 104.026 Pa and 2,175.141 Pa, an increase in its value tended to promote M2 polarization. Notably, when the G' was at 4620.253 Pa, the SHAP value dropped sharply. The SHAP value rebounded when the G' was at 6910.891 Pa, reflecting the promotion effect of G' on M2 polarization. These findings indicate that in designing hydrogel scaffolds aimed at promoting M2 polarization, the G' value should be kept away from 4620.253 Pa.

Figure 6E displays that when the R was between 0.307 and 0.654, a decrease in its value was apt to promote M2 polarization. However, when the R value was too low, e.g., at 0.143, an inhibitory effect on M2 polarization was seen. These results suggest that a moderate R is conducive to the promoting effect of hydrogel scaffolds on M2 polarization.

Figure 6F exhibits that when the PS was between 168.882 μm^2 and 27,850.340 μm^2 , an increase in its value was prone to

ML-guided hydrogel design for M2 polarization

promote M2 polarization. Conversely, the smallest value of PS at $88.923 \mu\text{m}^2$ showed an inhibitory effect on M2 polarization. These results indicate that an excessively low PS should not be taken into account in designing hydrogel scaffolds aimed at promoting M2 polarization.

The above results provide the specific ranges for all six properties to enhance the promotion of M2 polarization, serving as a foundation for enhancing the synergistic effects of physicochemical properties in hydrogel scaffolds.

3.5. Interactive effect analysis of the six physicochemical properties

With the independent effects of physicochemical properties investigated, the key point to enhance the synergistic effects on M2 polarization is to determine the interactive effects among the properties. Hence, the dependence plots of each physicochemical property with other properties were depicted based on the test set data (Figures 7-12).

For interactive effect quantification, each property was regarded as an interaction term to mediate the relationship between other physicochemical properties and their effects on M2 polarization. The interactive effects were reflected by changes in M2 polarization levels when the interaction term changed

while keeping other properties constant. Specifically, the interactive effect was visualized using the dependence plot of SHAP values for the physicochemical properties. For example, as shown in Figure 7D, when the value of P was controlled around 80%, three corresponding points were displayed with different colors. According to the legend of the blue-red gradient, um of these points were attributed to the change of interaction term, which in this case was G' . Consequently, by combining the SHAP value changes and the range of G' , the interactive effects of G' and P on M2 polarization were obtained.

For the optimization of the interactive effects, the independent effect of each physicochemical property on M2 polarization levels and the interactive effects of other physicochemical properties were combined to identify the value ranges of each physicochemical property that maximized M2 polarization levels. Then, the optimized combinations of physicochemical properties were generated.

3.5.1. Interactive effect analysis of p with other properties

Figure 7 shows the interactions of P with five physicochemical properties: G'' , SR, G' , R, PS, and IT. Among these features, IT, SR, and R did not exhibit obvious interactions with P on the test set (Figure 7A, C, and E). Figure 7B demonstrates

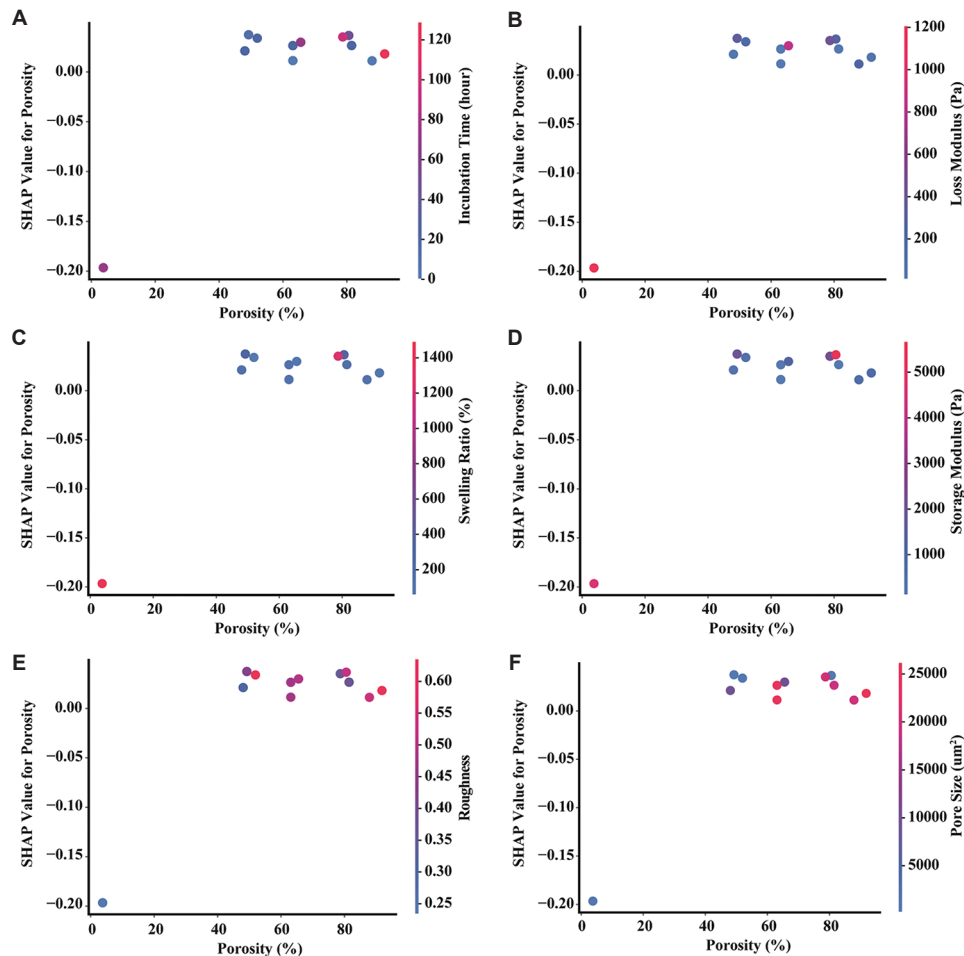


Figure 7. Dependence plots for SHAP values of porosity interacting with (A) incubation time, (B) loss modulus, (C) swelling ratio, (D) storage modulus, (E) roughness, and (F) pore size, reflecting potential interaction effects on M2 polarization of other physicochemical properties with porosity. Abbreviation: SHAP: Shapley additive explanations.

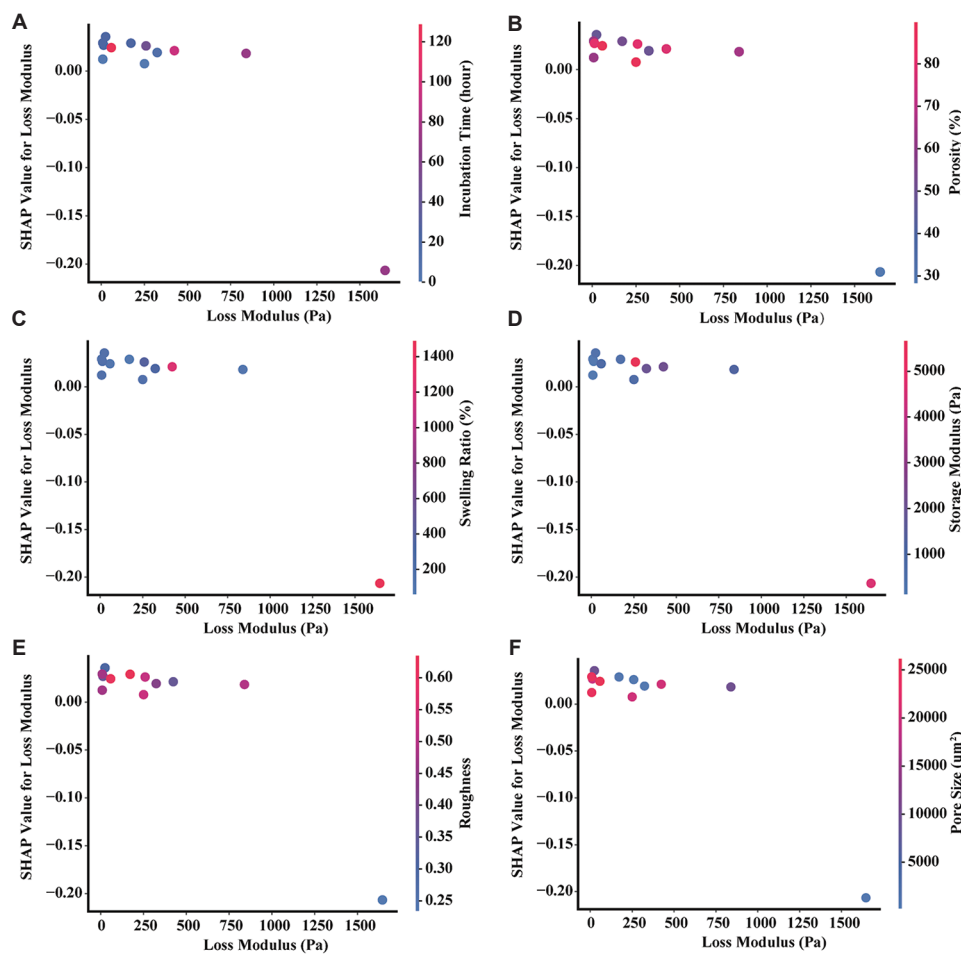


Figure 8. Dependence plot of SHAP value for loss modulus interacting with (A) incubation time, (B) porosity, (C) swelling ratio, (D) storage modulus, (E) roughness, and (F) pore size, reflecting potential interaction effects on M2 polarization of other physicochemical properties with loss modulus. Abbreviation: SHAP: Shapley additive explanations.

that when P was between 48.063% and 65.538%, increasing G'' within the range of 8.653 – 839.599 Pa enhanced the effect of P on M2 polarization. **Figure 7D** shows that when P was between 48.063% and 81.468%, increasing G' within the range of 104.026 – 6,910.891 Pa enhanced the effect of P on M2 polarization. **Figure 7E** exhibits that when P was between 48.063% and 81.468%, decreasing PS within the range of 88.923 – 24,668.131 μm^2 promoted the effect of P on M2 polarization.

These results suggest that G' , G'' , and PS have interactive effects with P in influencing M2 polarization within specific value ranges. They also imply that to enhance the synergistic effects of physicochemical properties for promoting M2 polarization, the following value ranges should be considered: P between 48.063% and 81.468%, G'' approaching 839.599 Pa, G' approaching 6,910.891 Pa, and PS approaching 88.923 μm^2 while ensuring that the independent effects of each physicochemical property are not significantly weakened.

3.5.2. Interactive effect analysis of G'' with other properties

Figure 8 displays the interactions of other features with G'' . Among these features, IT, P, SR, and G' did not exhibit obvious interactions with G'' on the test set (**Figure 8A-D**). **Figure 8E** demonstrates that when G'' was between 8.653 Pa and 423.729 Pa, decreasing R within the range of 0.307 – 0.654 enhanced

the effect of G'' on M2 polarization. **Figure 8F** shows that when G'' was between 8.653 Pa and 323.986 Pa, decreasing PS within the range of 88.923 – 27,850.340 μm^2 enhanced the effect of G'' on M2 polarization.

These results indicate that R and PS have interactive effects with G'' in influencing M2 polarization within specific value ranges. They also imply that to enhance the synergistic effects of physicochemical properties for promoting M2 polarization with G'' between 8.653 Pa and 323.986 Pa, it is rational to make R approaching 0.307 and PS approaching 27,850.340 μm^2 while ensuring that the independent effects of each physicochemical property are not significantly weakened.

3.5.3. Interactive effect analysis of SR with other properties

Figure 9 depicts the interactions of other features with SR. Unexpectedly, none of the features exhibited obvious interactions with SR on the test set (**Figures 9A-F**). This indicates that SR is generally regarded as an independent element in the process of enhancing the synergistic effects of physicochemical properties for promoting M2 polarization.

3.5.4. Interactive effect analysis of G' with other properties

Figure 10 demonstrates the interactions of other features with G' . Among these features, IT, P, G'' , SR, and R did

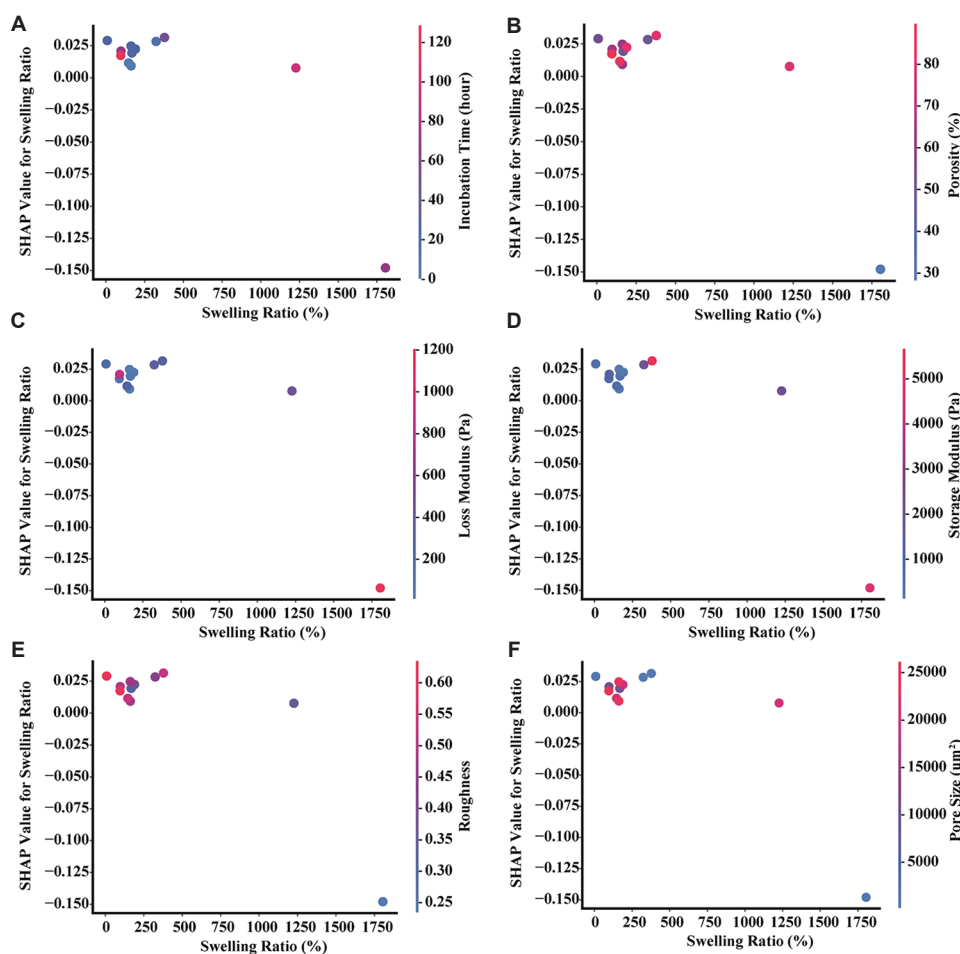


Figure 9. Dependence plots of SHAP values of swelling ratio interacting with (A) incubation time, (B) porosity, (C) loss modulus, (D) storage modulus, (E) roughness, and (F) pore size, reflecting potential interaction effects on M2 polarization of other physicochemical properties with swelling ratio. Abbreviation: SHAP: Shapley additive explanations.

not exhibit obvious interactions with G' on the test set (**Figure 10A-E**). **Figure 10F** shows that when G' was between 104.026 Pa and 834.586 Pa, increasing PS within the range of 357.735 – 27,850.340 μm^2 facilitated the effect of G' on M2 polarization.

These results suggest that PS has an interactive effect with G' in influencing M2 polarization within a specific value range. It also implies that to enhance the synergistic effects of physicochemical properties for promoting M2 polarization, especially with G' between 104.026 Pa and 834.586 Pa, the optimal choice is to set PS approaches 27,850.340 μm^2 while ensuring that the independent effects of each physicochemical property are not significantly weakened.

3.5.5. Interactive effect analysis of R with other properties

Figure 11 exhibits the interactions of other features with R. Among these features, IT, P, G'' , SR, and G' did not exhibit obvious interactions with R on the test set (**Figure 11A-E**). **Figure 11F** shows that when R was between 0.475 and 0.532, decreasing PS within the range of 168.882 – 24,668.131 μm^2 enhanced the effect of R on M2 polarization.

These results suggest that PS has an interactive effect with R in influencing M2 polarization within a specific value range.

Therefore, to enhance the synergistic effects of physicochemical properties for promoting M2 polarization with R between 0.475 and 0.532, it is reasonable to set PS approaches 168.882 μm^2 while ensuring that the independent effects of each physicochemical property are not significantly weakened.

3.5.6. Interactive effect analysis of PS with other properties

Figure 12 displays the interactions of other features with PS. Among these features, IT, P, G'' , and R did not exhibit obvious interactions with PS on the test set (**Figure 12A-C, and F**). **Figure 12D** demonstrates that when PS was between 88.923 μm^2 and 388.427 μm^2 , decreasing SR within the range of 8.372 – 1,804.511% enhanced the effect of PS on M2 polarization. **Figure 12E** shows that when PS was between 88.923 μm^2 and 357.735 μm^2 , decreasing G' within the range of 505.067 – 6,910.891 Pa enhanced the effect of PS on M2 polarization.

These results suggest that SR and G' have interactive effects with PS in influencing M2 polarization within specific value ranges. Therefore, to enhance the synergistic effects of physicochemical properties for promoting M2 polarization with PS between 88.923 μm^2 and 357.735 μm^2 , it is encouraged to set SR approaches 8.372% and G' approaches 505.067 Pa

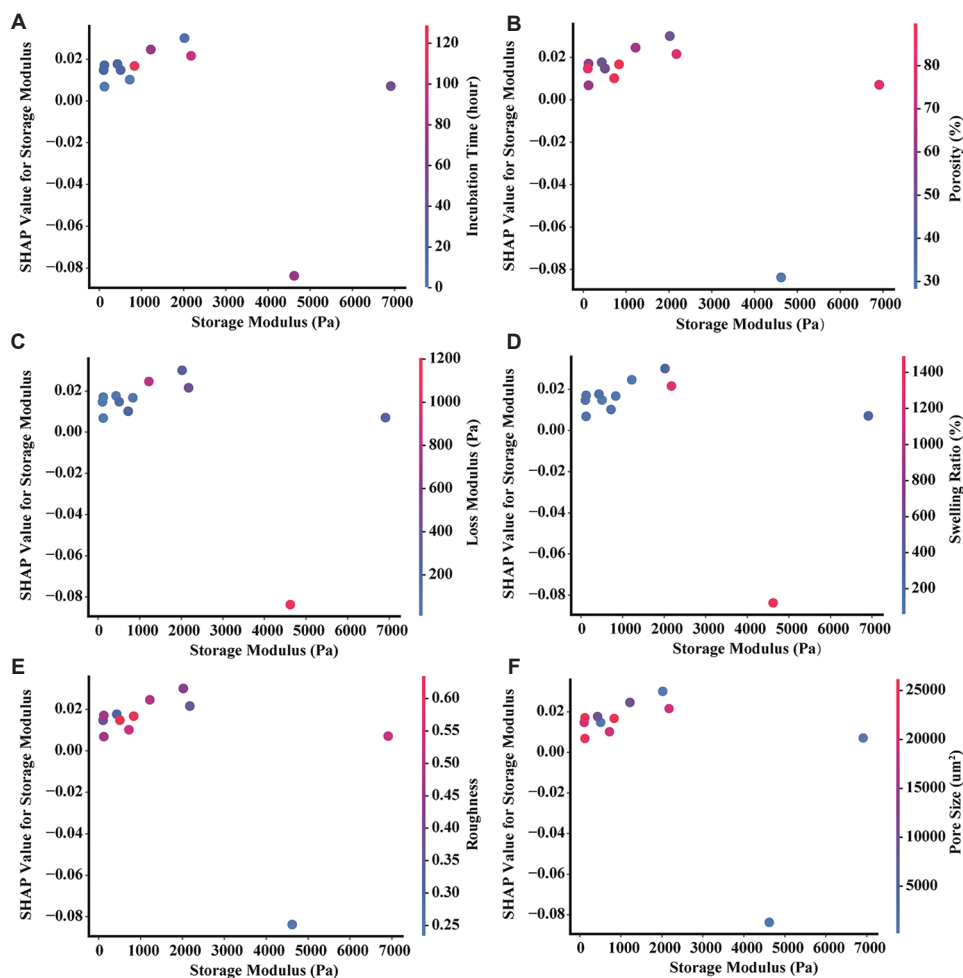


Figure 10. Dependence plots of SHAP values of storage modulus interacting with (A) incubation time, (B) porosity, (C) loss modulus, (D) swelling ratio, (E) roughness, and (F) pore size, reflecting potential interaction effects on M2 polarization of other physicochemical properties with storage modulus. Abbreviation: SHAP: Shapley additive explanations.

while ensuring that the independent effects of each property are not significantly weakened.

Overall, the specific ranges of all properties interacting with others to promote M2 polarization are listed, serving as another basis for enhancing the synergistic effects of physicochemical properties in hydrogel scaffolds.

3.6. Proposal of the IML-OPP strategy

As analyzed above, the importance ranking, independent effects, and interactive effects of the physicochemical properties in hydrogel scaffold on M2 polarization under the optimal RF model have been clearly demonstrated. Based on this, the IML-OPP strategy was proposed to enhance the synergistic effects of physicochemical properties. In summary, under different manufacturing conditions or application scenarios, the optimization process should be conducted step by step based on the importance ranking of the physicochemical properties. While optimizing each physicochemical property, both the independent and interactive effects must be considered in sequence to enhance M2 polarization comprehensively. This approach ensures that the potential rise in synergistic effects between properties does not come at the cost of diminishing

the independent effect of any single property, which could weaken the overall M2 polarization level. Ultimately, the various combinations of physicochemical properties, selected according to these principles, should be normalized and input into the optimal RF model, with multiple IT time points taken into account. This will allow for the preferential selection of combinations that can maintain the M2 polarization phenotype for longer periods.

To apply the strategy, suppose there was a demand to prepare a hydrogel scaffold with approximately 50% P and the function to promote M2 polarization. The first step was to consider optimizing the physicochemical property G'' , which has a higher importance ranking. For the independent effect of G'' , a decrease in its value significantly promoted M2 polarization when it fell between 839.599 Pa and 1,645.570 Pa. In addition, when P was set to 50%, increasing G'' within the range of 8.653 Pa – 839.599 Pa enhanced the promoting effect of P on M2 polarization. Considering both the independent and interactive effects, the optimal value for G'' was 839.599 Pa.

Once G'' was determined, the second property to optimize was SR. For the independent effect of SR, 377.815% was the value that maximized its effect on M2 polarization. Since there were

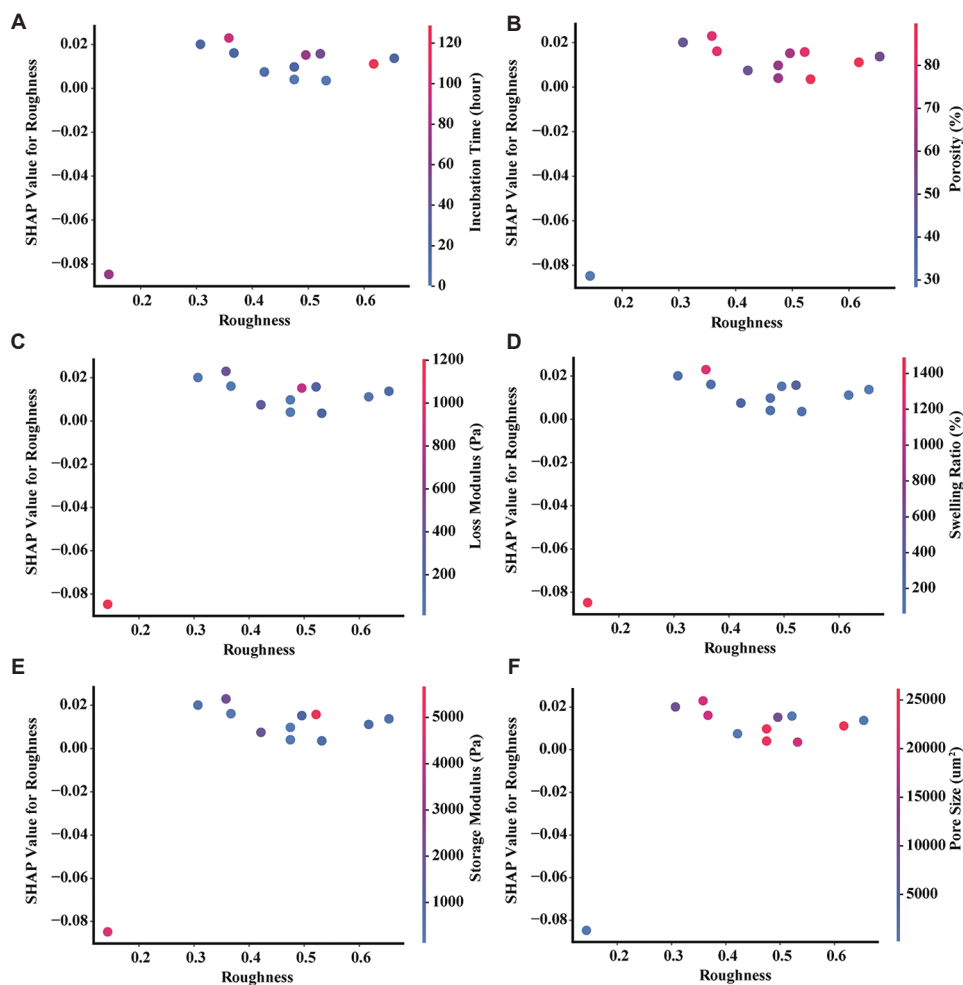


Figure 11. Dependence plots of SHAP values of roughness interacting with (A) incubation time, (B) porosity, (C) loss modulus, (D) swelling ratio, (E) storage modulus, and (F) pore size, reflecting potential interaction effects on M2 polarization of other physicochemical properties with roughness. Abbreviation: SHAP: Shapley additive explanations.

no significant interactions between SR and other properties, the optimal value for SR was set to 377.815%.

The third property to optimize was G' due to its importance ranking. When its value was between 104.026 Pa and 2,175.141 Pa, increasing G' tended to promote M2 polarization. On the other hand, when P was at 50%, increasing G' in the range of 104.026 Pa – 6,910.891 Pa tended to enhance the effect of P on M2 polarization. Notably, the independent effect of G' and its interaction with P showed a degree of conflict, indicating that further numerical testing was necessary to determine the optimal value. Therefore, G' was provisionally set to 2,175.141 Pa or 6,910.891 Pa, pending further evaluation using the optimal RF model.

As the fourth in the importance ranking, R was optimized subsequently. When it was between 0.307 and 0.654, decreasing R inclined to promote M2 polarization. Given that there is no significant interaction between R and other physicochemical properties under the current conditions, the value of R was set to 0.307.

Finally, the determination of PS completed the optimization process. Interestingly, although PS contributed less to M2

polarization independently, it exhibited interactions with multiple physicochemical properties, leading to variable interactive effects depending on the context. Given the complexity of its relationship with M2 polarization, the inflection point of its independent effect, 168.882 μm^2 , was selected as the optimal value. This choice balanced the independent and interactive effects of PS, thereby minimizing any potential negative impact on M2 polarization.

After determining the values for the six physicochemical properties, the combinations with two candidate G' values were matched with six IT values – 12 h, 24 h, 48 h, 72 h, 96 h, and 168 h – resulting in 12 feature combinations. These combinations were normalized and input into the optimal RF model for prediction. Based on the comparison of target classes, the optimal combinations could be selected. Notably, all 12 combinations were predicted to achieve target 2, indicating that under the constraint of P being 50%, the optimized physicochemical property combinations of hydrogel scaffolds were capable of promoting M2 polarization synergistically for a long duration.

Similarly, two other optimized combinations were provided as examples under conditions where two or three properties were limited. For example, if G' was set at 2,000 Pa and G''

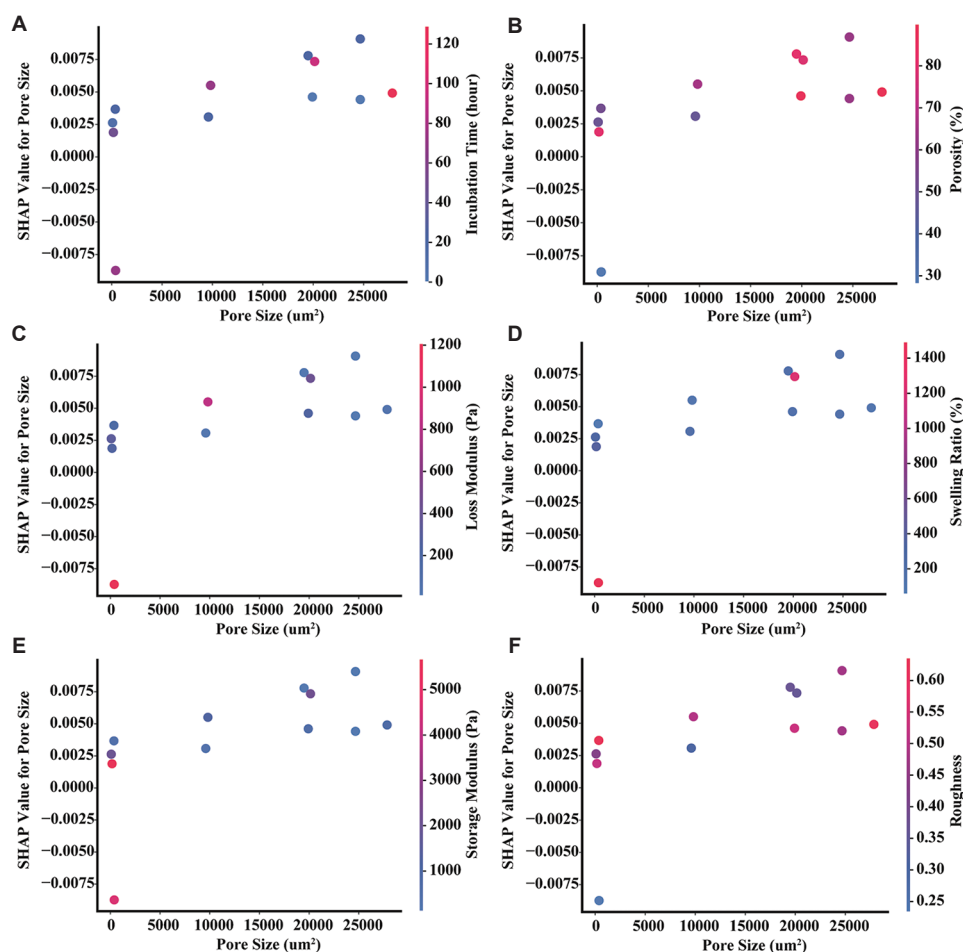


Figure 12. Dependence plots of SHAP values of pore size interacting with (A) incubation time, (B) porosity, (C) loss modulus, (D) swelling ratio, (E) storage modulus, and (F) roughness, reflecting potential interaction effects on M2 polarization of other physicochemical properties with pore size. Abbreviation: SHAP: Shapley additive explanations.

at 500 Pa, the optimal values for other properties, calculated based on the IML-OPP strategy, were determined as follows: P: 81.468%, SR: 377.815%, R: 0.307, and PS: 168.882 μm^2 . In another case, when SR was limited to 1,000%, R to 0.5, and PS to 100 μm^2 , the optimal values of other properties were as follows: P: 81.468%, G': 2,175.141 Pa, and G'': 839.599 Pa.

As presented in **Table 3**, three combinations of physicochemical properties were provided as examples, confirming the robustness and universality of the IML-OPP strategy.

4. Discussion

Given the complexity and independence of various biomedical issues, a method that can precisely, efficiently, and uniformly address synergistic multi-factor interactions has long been lacking. Traditional methods, such as one-factor orthogonal experiments, have inherent limitations when conducting multi-factor comparisons with synergistic effects, often leading to tremendous time and effort consumption. As a result, there is an urgent need for novel methods. IML, a modeling method of information technology to explain relationships among multiple factors in quantification, has drawn significant attention in many fields nowadays.¹⁸ In biomedicine, IML holds a promise to address multi-factor biomedical issues in a fast, accurate, and uniform manner. For

example, IML has been used to identify the comprehensive hazard level of multiple risk factors and define thresholds for the onset, progression, and regression of epidemic diseases. Its accuracy and efficiency contribute to the development of individualized applications of prevention schemes.^{29,30} Besides, IML is applied to construct quantitative relationships between overall signals of multiple images and scores reflecting levels of diseases in medical imaging and pathology. By leveraging IML, images can more accurately identify lesions and exclude suspicious signals, thus reducing misdiagnosis and the rates of overlooked conditions.³¹ Moreover, IML has been utilized to explain how multiple manufacturing processes, such as the concentrations of components, collectively influence scaffold properties, including stiffness, degradation rate, and antibacterial ability. This provides a standardized framework for specific scaffold design.^{32,33} As discussed, IML's ability to illustrate the synergistic effects of multiple factors on specific biomedical outcomes highlights its potential application in addressing the unresolved issue of enhancing the synergistic effects of multiple physicochemical properties in hydrogel scaffolds on M2 polarization.

To employ IML to enhance the synergistic effects of multiple properties on M2 polarization, the IML-OPP strategy was developed in this study. Unlike the conventional practice

ML-guided hydrogel design for M2 polarization

in IML-related research, where a single IML model was constructed, assessed, and interpreted in a relatively intuitive manner, this strategy incorporated both the comparison among multiple models and the interpretation based on the SHAP algorithm for the 1st time in the context of scaffold design in tissue engineering. As shown in **Figures 3 and 4**, the comparison among multiple models was performed to select the most suitable IML models for capturing the relationship between physicochemical properties and M2 polarization levels. Subsequently, the interpretation based on the SHAP algorithm was employed to derive optimized combinations through expected target classes, as illustrated in **Figures 5-12**. Without any of the two steps, the IML-OPP strategy could not be successfully established. Furthermore, the sequential execution of these two steps could be extended to constructing other relationships between scaffold parameters and cellular behaviors in tissue engineering, offering a universal methodological solution for the quantitative design of tissue engineering scaffolds from the perspective of methodological innovation.

Besides the methodological innovation by the construction of the IML-OPP strategy, this work stands out in its comprehensive measurement of M2 polarization compared with most current studies investigating macrophage polarization. As is universally acknowledged, there are various molecular indicators for M2 polarization, including surface antigens, secreting proteins, and intracellular enzymes, all of which can represent the levels of polarization.² However, researchers often select different indicators based on specific experimental conditions and preferences, and even the same indicator may be measured using different techniques across laboratories. Therefore, it is challenging to perform horizontal comparisons among studies to assess differing levels of M2 polarization. To address this challenge, this study employed a standardized measurement of M2 polarization across all samples derived from different initial studies, enabling a comprehensive and standardized comparison. As described in the section data preprocessing, indicators obtained from different experimental techniques were normalized into classes to eliminate disparities arising from measurement variability. Moreover, by averaging the classes of diverse indicators representing polarization levels, the analysis reduced the influence of missing or outlier values. Importantly, the inclusion of M1-related indicators, whose trends typically oppose those of M2-related indicators, further enhanced the generalizability of the assessment of M2 polarization. From an application point of view, this integrated consideration of M1 and M2 indicators provides a more holistic view of the inflammatory status within the post-injury microenvironment *in vivo*, thereby enhancing the clinical translational potential of hydrogel scaffolds designed using the IML-OPP strategy.

The construction and application framework of the IML-OPP strategy is universal. In a narrower context, considering that the six physicochemical properties investigated are commonly present across hydrogel scaffolds, and that the selected ML models are well-established in the biomedical field, this systematic framework can readily be applied to quantify

relationships between physicochemical properties of hydrogel scaffolds and a range of cytological features, such as macrophage M1 polarization levels, stem cell proliferative capacity, or even *in vivo* indices like antibacterial efficacy.³⁴⁻³⁸ This approach enables the formulation of IML-guided optimization strategies to address the combinatorial effects of physicochemical properties on specific cytobiological behaviors.

From a broader methodological perspective, the comprehensive workflow established in this study – encompassing public data collection, dataset construction, model training and comparison, interpretability analysis, and optimization strategy development – holds significant potential for wider application. Indeed, this framework is not limited to studies of the physicochemical properties of hydrogel scaffolds. Provided that the reliability of original research, representativeness of sample selection, and rationality of data processing are rigorously upheld, this framework could be extended to other types of scaffolds or expanded to include additional factors influencing cytological characteristics – such as scaffold material composition, synthesis protocols, and incorporation of bioactive factors. Such modifications would not compromise the methodological integrity or impede the progression of the study.

In addition, it is worth noting that the IML-OPP strategy has the potential for future upgrades. This is primarily because the optimal IML model proposed in this study can be continuously optimized over time. Unlike conventional IML-related studies in tissue engineering, where training data are mainly acquired from experiments conducted by the researcher team, this study, as illustrated in **Figure 2**, constructed its dataset from a wide range of public literature. This approach not only enhances the generalization of the IML models but also provides opportunities for future data integration. As research on leveraging the physicochemical properties of hydrogel scaffolds to promote M2 polarization continues to expand, additional samples will become available for inclusion in the dataset applied in the ML models. The continuous emergence of new samples is expected to facilitate further improvements in data mining, feature selection, and target assignment, providing ongoing impetus for updating the IML-OPP strategy.

With regard to study limitations, firstly, the data collection process in this study was inherently subject to selection bias due to its complete dependence on literature. To mitigate this, the dataset was carefully curated to maximize diversity and representativeness by including a broad range of samples. Furthermore, samples exhibiting significant variations in confounding factors unrelated to physicochemical properties were systematically excluded based on a rigorous review of the literature. However, it was important to recognize that potential bias may persist due to ambiguities in literature descriptions, subjective tendencies of data collectors, and variations in experimental conditions across studies. Consequently, while the quantitative model and optimization strategies proposed in this study demonstrated promising predictive capabilities, their performances could be further enhanced. Nevertheless, although the limitation of selection bias was inevitable, the methodological innovation in the construction and application of the IML-OPP strategy was

Table 1. General description for 21 interpretable machine learning models

Model	Strengths	Weaknesses	Hyperparameters to be optimized
KNN ³⁹	Simple principle, suitability for multi-classification problems, insensitivity to outliers	Complex calculation, high requirements for memory and data distribution	'n_neighbors' 'weights' 'distance'
XGBoost ⁴⁰	Parallel computing, fast training, accurate prediction, good feature interpretability	Complex parameter tuning, sensitivity to outliers, tendency to overfitting in small sample datasets	'learning_rate' 'max_depth' 'n_estimators'
CatBoost ⁴¹	Excellent performance on processing large-scale datasets with categorical features	Requirements for large computing resources, sensitivity to outliers	'depth' 'iterations' 'learning_rate'
LGBM classifier ⁴²	Improved scalability and accuracy compared to traditional tree-boosting algorithms	Poor interpretability, tendency to overfitting, difficulty in incremental training	'colsample_bytree' 'learning_rate' 'n_estimators' 'subsample'
DT ⁴³	Facility in understanding and interpretation, simple data preprocessing, ability to learn non-linear relationships	Sensitivity to noise, tendency to overfitting	'criterion' 'max_depth' 'min_samples_leaf' 'min_samples_split'
RF ⁴⁴	High accuracy, strong robustness, wide applicability	Complex model, difficulty in interpreting, long training time	'max_depth' 'min_samples_leaf' 'min_samples_split' 'n_estimators'
Extra trees ⁴⁵	Reduction in model variance, low overfitting risk, improved model robustness	Model instability from excessive randomness, increased risk of underfitting	'max_depth' 'min_samples_leaf' 'min_samples_split' 'n_estimators'
RGF classifier ⁴⁶	Excellent performance on high-dimensional and large-scale datasets, high accuracy and robustness, low memory consumption, simple parameter tuning	Slow training speed, long prediction time, poor performance on non-linear problems	'algorithm' 'l2' 'max_leaf' 'min_samples_leaf'
NN ⁴⁷	Strong adaptability, high flexibility, and good generalization ability	Poor interpretability, high overfitting risk, difficulty in hyperparameter adjustment	'lr' 'hidden_size' 'Batch size' 'Activation function' 'num_epochs' 'Stochastic optimization'
Logistic regression ⁴⁸	Strong interpretability, output form of probability, suitability for sparse data	Poor performance on handling non-linear problems, tendency to underfitting on complex data structures	'C' 'penalty': 'l2'
SVM ⁴⁹	Good generalization ability, strong robustness, suitability for high-dimensional space and linearly separable problems	High computational complexity, large memory consumption, unsuitability for complex, non-linear, large-scale, and multi-class problems	'C' 'gamma' 'kernel'
Linear SVC ⁴⁹	low memory footprint, simple parameter adjustments	Poor performance on non-linear and non-convex feature space cases	'C' 'loss' 'penalty'
LDA ⁵⁰	Low computational cost, low overfitting risk, suitability for linear high-dimensional datasets	Poor performance on non-linear, non-Gaussian, and unbalanced class datasets	'shrinkage' 'solver'
QDA ⁵¹	Flexibility in fitting non-linear relationships	High requirements for parameter estimation, sensitivity to outliers, poor performance on small samples, high computational complexity, difficulty in handling high-dimensional data	'reg_param'
Label propagation ⁵²	Model independent of feature space, ability to achieve overall prediction with a small number of real-labeled samples, strong scalability for large-scale datasets	Limitation in graph structure selection and handling of isolated nodes	'gamma' 'kernel' 'n_neighbors'
GPC ⁵³	Superiority in uncertainty estimation, good performance on small samples and non-linear problems	High computational complexity, unsuitability for large-scale complex datasets, poor performance on high-dimensional space	'kernel'
Ridge classifier ⁵⁴	Good interpretability, suitability for handling overfitting and collinearity problems	Unsuitability for sparse datasets, high requirements for data distribution	'alpha' 'solver'

(Cont'd...)

Table 1. (Continued)

Model	Strengths	Weaknesses	Hyperparameters to be optimized
MLP Classifier ⁴⁷	Strong fitting ability, high adaptability, excellent performance on handling large-scale and complex data, facility in multi-classification problems	High requirements for size and hyperparameter adjustment, poor interpretability	'alpha' 'hidden_layer_sizes'
Gaussian NB ⁵⁵	Suitability for high-dimensional and small-scale datasets with missing values	Limitation in independence assumptions and distribution requirements, difficulty in handling feature correlations, tendency to prediction bias on unbalanced classes	'var_smoothing'
Bernoulli NB ⁵⁶	Suitability for sparse data and text classification processing	Difficulty in handling interactions between features, limitation in independence assumptions and distribution requirements	'alpha' 'binarize' 'fit_prior'
PAC ⁵⁷	Ability to gradually adapt to new data without repeated model training	Performance depends on parameter selection, tendency to overfitting with continuous addition of new data	'C' 'fit_intercept'

Abbreviations: Bernoulli NB: Bernoulli Naive Bayes; CatBoost: Categorical boosting; DT: Decision tree; Extra Trees: Extremely randomized trees; Gaussian NB: Gaussian Naive Bayes; GPC: Gaussian process classifier; KNN: K-nearest neighbors; LDA: Linear discriminant analysis; LGBM: Light gradient boosting machine; Linear SVC: Linear support vector classification; MLP: Multi-layer perceptron; NN: Neural network; PAC: Passive aggressive classifier; QDA: Quadratic discriminant analysis; RF: Random forest; RGF: Regularized greedy forest; SVM: Support vector machine; XGBoost: Extreme gradient boosting.

Table 2. Outcomes of hyperparameter optimization for 21 interpretable machine learning models

Model	Optimized hyperparameters
KNN	'n_neighbors': 3, 'weights': 'uniform'
XGBoost	'learning_rate': 0.01, 'max_depth': 3, 'n_estimators': 50
CatBoost	'depth': 4, 'iterations': 50, 'learning_rate': 0.2
LGBM classifier	'colsample_bytree': 0.8, 'learning_rate': 0.01, 'n_estimators': 50, 'subsample': 0.8
DT	'criterion': 'entropy', 'max_depth': None, 'min_samples_leaf': 1, 'min_samples_split': 2
RF	'max_depth': None, 'min_samples_leaf': 1, 'min_samples_split': 2, 'n_estimators': 50
Extra Trees	'max_depth': None, 'min_samples_leaf': 2, 'min_samples_split': 10, 'n_estimators': 200
RGF classifier	'algorithm': 'RGF', 'l2': 0.1, 'max_leaf': 1000, 'min_samples_leaf': 10
NN	'lr': 0.001, 'hidden_size': 64, 'Batch size': 64, 'num_epochs': 10
Logistic regression	'C': 10, 'penalty': 'l2'
SVM	'C': 10, 'gamma': 'scale', 'kernel': 'linear'
Linear SVC	'C': 1, 'loss': 'squared_hinge', 'penalty': 'l2'

(Cont'd...)

Table 2. (Continued)

Model	Optimized hyperparameters
LDA	'shrinkage': 'auto', 'solver': 'lsqr'
QDA	'reg_param': 0.0
Label propagation	'gamma': 0.1, 'kernel': 'knn', 'n_neighbors': 3
GPC	'kernel': RBF (length_scale=1)
Ridge Classifier	'alpha': 0.1, 'solver': 'auto'
MLP classifier	'alpha': 0.0001, 'hidden_layer_sizes': (50,50)
Gaussian NB	'var_smoothing': 1e-09
Bernoulli NB	'alpha': 0.1, 'binarize': 0.5, 'fit_prior': False
PAC	'C': 1, 'fit_intercept': False

Abbreviations: Bernoulli NB: Bernoulli Naive Bayes; CatBoost: Categorical boosting; DT: Decision tree; Extra Trees: Extremely randomized trees; Gaussian NB: Gaussian Naive Bayes; GPC: Gaussian process classifier; KNN: K-nearest neighbors; LDA: Linear discriminant analysis; LGBM: Light gradient boosting machine; Linear SVC: Linear support vector classification; MLP: Multi-layer perceptron; NN: Neural network; PAC: Passive aggressive classifier; QDA: Quadratic discriminant analysis; RF: Random forest; RGF: Regularized greedy forest; SVM: Support vector machine; XGBoost: Extreme gradient boosting.

significant. Based on the framework of IML-OPP, it can be anticipated that reducing selection bias will require expanding the sample size and improving dataset consistency, which will depend on the continuous generation of high-quality primary research data.

In addition, potential bias arose from the diversity of original research methods used to generate the target data. As outlined in the methodology section, to maximize the scale of the dataset, samples included in this study were derived from multiple M2 polarization evaluation methods, including WB, qPCR, FC, and ELISA. In general, these methods measure the contents of the same substances and usually show consistent expression trends. However, although these methods exhibit a certain degree of correlation in reflecting the overall trend

Table 3. Three optimized combinations generated by the interpretable machine learning-driven optimization of physicochemical properties strategy

Optimized combination	G' (Pa)	G'' (Pa)	PS (μm^2)	P (%)	SR (%)	R
1	104.026/2,175.141	839.599	377.815	50	168.882	0.307
2	2,000	500	377.815	81.468	168.882	0.307
3	2,175.141	839.599	100	81.468	1,000	0.5

Abbreviations: G': Storage modulus; G'': Loss modulus; P: Porosity; PS: Pore size; R: Roughness; SR: Swelling ratio.

of macrophage polarization, diversity among them exists. Specifically, ELISA is widely recognized for its precision and reproducibility in quantifying trace amounts of proteins. In contrast, WB, qPCR, and FC being semi-quantitative methods with relatively lower measurement accuracy and more complex experimental procedures, may yield fluctuating quantitative results. Given the need for a sample size as large as possible, generating a comprehensive index to evaluate M2 polarization was the best option, although it inevitably introduced bias. Nevertheless, this bias was acceptable due to rational statistical processing. Specifically, various classification labels were assigned to samples based on their corresponding evaluation methods to facilitate the definition of different polarization levels. Furthermore, by averaging the results across methods, the variations among evaluation techniques were balanced, ensuring that the classification labels for each sample were more generalizable and representative. Indeed, the comprehensive evaluation methods employed in this study played a critical role in developing the optimization strategy.

Three optimized combinations of physicochemical properties were provided as examples to demonstrate how to use the IML-OPP strategy in hydrogel scaffold design. These examples showed how, under the conditions of one, two, or three properties being confined, the other properties should be orderly determined with balanced independent and interactive effects. In this way, the robustness and universality of the IML-OPP strategy were validated. It is anticipated that the strategy will assist in the efficient and precise design of hydrogel scaffolds in the future, thereby improving the synergistic effects of physicochemical properties on M2 polarization.

5. Conclusions

In this study, three optimized combinations of physicochemical properties in hydrogel scaffolds were provided using a novel strategy called IML-OPP. The IML-OPP strategy offers innovative and comprehensive theoretical guidance for designing hydrogel scaffolds that promote M2 polarization, thereby facilitating the clinical translation of these hydrogel scaffolds.

Acknowledgement

We thank all researchers whose study data were included in this study for their contributions to the public information on hydrogel scaffolds.

Financial support

This work was supported by the National Natural Science Foundation of China (No. 52003149), the Natural Science Foundation of Shanghai (No. 24ZR1464000), the Funding of Shanghai Science and Technology Commission Project (No. 22Y11912000), the Funding of Orthopedic Priority Speciality of Changning District (No. 20231002), the Funding of Minimally Invasive Spine Surgery Research Center of Shanghai Jiao Tong University (No. 2021JCPT03), the Laboratory Open Fund of Key Technology and Materials in Minimally Invasive Spine Surgery (Tongren Hospital, Shanghai

Jiao Tong University School of Medicine) (No. 2024JZWC-ZDA02), and the Star-up Funds for Talent Introduction (Tongren Hospital, Shanghai Jiao Tong University School of Medicine) (No. TR2024RC17).

Conflicts of interest statement

The authors declared no potential conflicts of interest with respect to the research, authorship, and/or publication of this work.

Author contributions

Conceptualization: ZH, YH, and ZC; *Data curation:* ZH, YH, ZC, TT, and YL; *Funding acquisition:* XY; *Project administration:* PX and XY; *Resources:* ZH, YH, ZC, TT, and YL; *Supervision:* PX and XY; *Writing – original draft:* ZH, YH, and ZC; *Writing – editing & review:* ZH, YH, ZC, YC, and LX. All authors read and approved the final version of the manuscript.

Ethics approval and consent to participate

Not applicable.

Consent for publication

Not applicable.

Availability of data

The dataset included in this work is publicly available in the literature. **Table S1** presents information on features and targets for each sample.

Open access statement

This is an open access journal, and articles are distributed under the terms of the Creative Commons Attribution-NonCommercial-ShareAlike 4.0 License, which allows others to remix, tweak, and build on the work non-commercially, as long as appropriate credit is given and the new creations are licensed under the identical terms.

References

- Zaid A, Ariel A. Harnessing anti-inflammatory pathways and macrophage nano delivery to treat inflammatory and fibrotic disorders. *Adv Drug Deliv Rev.* 2024;207:115204. doi: 10.1016/j.addr.2024.115204
- Chen S, Saeed A, Liu Q, et al. Macrophages in immunoregulation and therapeutics. *Signal Transduct Target Ther.* 2023;8:207. doi: 10.1038/s41392-023-01452-1
- Long A, Kleiner A, Looney RJ. Immune dysregulation. *J Allergy Clin Immunol.* 2023;151:70-80. doi: 10.1016/j.jaci.2022.11.001
- Alvarez MM, Liu JC, Trujillo-de Santiago G, et al. Delivery strategies to control inflammatory response: Modulating M1-M2 polarization in tissue engineering applications. *J Control Release.* 2016;240:349-363. doi: 10.1016/j.jconrel.2016.01.026
- Martin KE, García AJ. Macrophage phenotypes in tissue repair and the foreign body response: Implications for biomaterial-based regenerative medicine strategies. *Acta Biomater.* 2021;133:4-16. doi: 10.1016/j.actbio.2021.03.038
- Tu Z, Chen M, Wang M, et al. Engineering bioactive M2 macrophage-polarized anti-inflammatory, antioxidant, and antibacterial scaffolds for rapid angiogenesis and diabetic wound repair. *Adv Funct Mater.* 2021;31:2100924. doi: 10.1002/adfm.202100924
- Fisher LE, Kämmerling L, Alexander MR, Ghaemmaghami AM. Immune-instructive materials as new tools for immunotherapy. *Curr Opin Biotechnol.* 2022;74:194-203. doi: 10.1016/j.copbio.2021.11.005
- Jain N, Moeller J, Vogel V. Mechanobiology of macrophages: How physical factors coregulate macrophage plasticity and phagocytosis. *Annu Rev Biomed Eng.* 2019;21:267-297.

- doi: 10.1146/annurev-bioeng-062117-121224
9. Li J, Ke H, Lei X, *et al.* Controlled-release hydrogel loaded with magnesium-based nanoflowers synergize immunomodulation and cartilage regeneration in tendon-bone healing. *Bioact Mater.* 2024;36:62-82.
doi: 10.1016/j.bioactmat.2024.02.024
 10. Byun H, Han Y, Kim E, *et al.* Cell-homing and immunomodulatory composite hydrogels for effective wound healing with neovascularization. *Bioact Mater.* 2024;36:185-202.
doi: 10.1016/j.bioactmat.2024.02.029
 11. Teng YY, Zou ML, Liu SY, *et al.* Dual-action icariin-containing thermosensitive hydrogel for wound macrophage polarization and hair-follicle neogenesis. *Front Bioeng Biotechnol.* 2022;10:902894.
doi: 10.3389/fbioe.2022.902894
 12. Zhao T, Chen L, Yu C, *et al.* Effect of injectable calcium alginate-amelogenin hydrogel on macrophage polarization and promotion of jawbone osteogenesis. *RSC Adv.* 2024;14:2016-2026.
doi: 10.1039/d3ra05046g
 13. Li F, Liu T, Liu X, *et al.* *Ganoderma lucidum* polysaccharide hydrogel accelerates diabetic wound healing by regulating macrophage polarization. *Int J Biol Macromol.* 2024;260:129682.
doi: 10.1016/j.ijbiomac.2024.129682
 14. Lv L, Xie Y, Li K, *et al.* Unveiling the mechanism of surface hydrophilicity-modulated macrophage polarization. *Adv Healthc Mater.* 2018;7:e1800675.
doi: 10.1002/adhm.201800675
 15. Abaricia JO, Shah AH, Chaubal M, Hotchkiss KM, Olivares-Navarrete R. Wnt signaling modulates macrophage polarization and is regulated by biomaterial surface properties. *Biomaterials.* 2020;243:119920.
doi: 10.1016/j.biomaterials.2020.119920
 16. Frey DD, Engelhardt F, Greitzer EM. A role for "one-factor-at-a-time" experimentation in parameter design. *Res Eng Design.* 2003;14:65-74.
doi: 10.1007/s00163-002-0026-9
 17. Gu J, Gao C, Wang L. The evolution of artificial intelligence in biomedicine: Bibliometric analysis. *JMIR AI.* 2023;2:e45770.
doi: 10.2196/45770
 18. Rudin C, Chen C, Chen Z, Huang H, Semenova L, Zhong C. Interpretable machine learning: Fundamental principles and 10 grand challenges. *Stat Surv.* 2022;16: 1-85.
doi: 10.1214/21-ss133
 19. Cho YR, Kang M. Interpretable machine learning in bioinformatics. *Methods.* 2020;179:1-2.
doi: 10.1016/j.jymeth.2020.05.024
 20. Chen, X, Li, Y, Li, X, *et al.* An interpretable machine learning prognostic system for locoregionally advanced nasopharyngeal carcinoma based on tumor burden features. *Oral Oncol.* 2021;118:105335.
doi: 10.1016/j.oraloncology.2021.105335
 21. Alabi RO, Almangush A, Elmusrati M, Leivo I, Mäkitie AA. An interpretable machine learning prognostic system for risk stratification in oropharyngeal cancer. *Int J Med Inform.* 2022;168:104896.
doi: 10.1016/j.ijmedinf.2022.104896
 22. Echezarreta-López MM, Landin M. Using machine learning for improving knowledge on antibacterial effect of bioactive glass. *Int J Pharm.* 2013;453:641-647.
doi: 10.1016/j.ijpharm.2013.06.036
 23. Rafieyan S, Vasheghani-Farahani E, Baheiraei N, Keshavarz H. MLATE: Machine learning for predicting cell behavior on cardiac tissue engineering scaffolds. *Comput Biol Med.* 2023;158:106804.
doi: 10.1016/j.combiomed.2023.106804
 24. Kinney JB, Atwal GS. Equitability, mutual information, and the maximal information coefficient. *Proc Natl Acad Sci USA.* 2014;111:3354-3359.
doi: 10.1073/pnas.1309933111
 25. Goecks J, Jalili V, Heiser LM, Gray JW. How machine learning will transform biomedicine. *Cell.* 2020;181:92-101.
doi: 10.1016/j.cell.2020.03.022
 26. Guo JL, Januszyn M, Longaker MT. Machine learning in tissue engineering. *Tissue Eng Part A.* 2023;29:2-19.
doi: 10.1089/ten.TEA.2022.0128
 27. Raschka, S. Model evaluation, model selection, and algorithm selection in machine learning. *ArXiv.* 2018.
doi: 10.48550/arXiv.1811.12808
 28. Ponce-Bobadilla AV, Schmitt V, Maier CS, Mensing S, Stodtmann S. Practical guide to SHAP analysis: Explaining supervised machine learning model predictions in drug development. *Clin Transl Sci.* 2024;17:e70056.
doi: 10.1111/cts.70056
 29. Li X, Zhao Y, Zhang D, *et al.* Development of an interpretable machine learning model associated with heavy metals' exposure to identify coronary heart disease among US adults via SHAP: Findings of the US NHANES from 2003 to 2018. *Chemosphere.* 2023;311:137039.
doi: 10.1016/j.chemosphere.2022.137039
 30. Liu T, Siegel E, Shen D. Deep learning and medical image analysis for COVID-19 diagnosis and prediction. *Annu Rev Biomed Eng.* 2022;24:179-201.
doi: 10.1146/annurev-bioeng-110220-012203
 31. Calderaro J, Žigutytė L, Truhn D, Jaffe A, Kather JN. Artificial intelligence in liver cancer - new tools for research and patient management. *Nat Rev Gastroenterol Hepatol.* 2024;21:585-599.
doi: 10.1038/s41575-024-00919-y
 32. Karaoglu IC, Kebabci AO, Kizilel S. Optimization of gelatin methacryloyl hydrogel properties through an artificial neural network model. *ACS Appl Mater Interfaces.* 2023;15:44796-44808.
doi: 10.1021/acsami.3c12207
 33. Liu W, Zhang Y, Lyu Y, Bosiakov S, Liu Y. Inverse design of anisotropic bone scaffold based on machine learning and regenerative genetic algorithm. *Front Bioeng Biotechnol.* 2023;11:1241151.
doi: 10.3389/fbioe.2023.1241151
 34. Ghalavand M, Moradi-Chaleshtori M, Dorostkar R, Mohammadi-Yeganeh S, Hashemi SM. Exosomes derived from rapamycin-treated 4T1 breast cancer cells induced polarization of macrophages to M1 phenotype. *Biotechnol Appl Biochem.* 2023;70:1754-1771.
doi: 10.1002/bab.2473
 35. Zhang H, Qin C, Shi Z, *et al.* Bioprinting of inorganic-biomaterial/neural-stem-cell constructs for multiple tissue regeneration and functional recovery. *Natl Sci Rev.* 2024;11:nwae035.
doi: 10.1093/nsr/nwae035
 36. Wang W, Cui Y, Wei X, *et al.* CuCo(2)O(4) nanoflowers with multiple enzyme activities for treating bacterium-infected wounds via cuproptosis-like death. *ACS Nano.* 2024;18:15845-15863.
doi: 10.1021/acsnano.4c02825
 37. Hu Z, Shan J, Jin X, *et al.* Nanoarchitectonics of *in situ* antibiotic-releasing acicular nanozymes for targeting and inducing cuproptosis-like death to eliminate drug-resistant bacteria. *ACS Nano.* 2024;18:24327-24349.
doi: 10.1021/acsnano.4c06565
 38. Sun Y, Zhang W, Luo Z, *et al.* ZnO-CuS/F127 hydrogels with multienzyme properties for implant-related infection therapy by inhibiting bacterial arginine biosynthesis and promoting tissue repair. *Adv Funct Mater.* 2024;35(8):2415778.
doi: 10.1002/adfm.202415778
 39. Taunk K, De S, Verma S, Swetapadma A. A Brief Review of Nearest Neighbor Algorithm for Learning and Classification. In: *Proceedings of the 2019 International Conference on Intelligent Computing and Control Systems (ICCS)*. Madurai, India: IEEE; 2019. p. 1255-1260.
doi: 10.1109/ICCS45141.2019.9065747
 40. Chen T, Guestrin C. XGBoost. In *Proceedings of the 22nd ACM SIGKDD International Conference on Knowledge Discovery and Data Mining.* 2016. p. 785-794.
doi: 10.1145/2939672.2939785
 41. Prokhorenkova L, Gusev G, Vorobev A, Dorogush AV, Gulin A. CatBoost: Unbiased Boosting with Categorical Features. In: *Advances in Neural Information Processing Systems 31 (NIPS 2018)*. Vol. 31. 2018. p. 6639-6649.
 42. Ke GL, Meng Q, Finley T, *et al.* LightGBM: A Highly Efficient Gradient Boosting Decision Tree. In: *Advances in Neural Information Processing Systems 30 (NIPS 2017)*. Vol. 30. 2017. p. 3149-3157.
 43. Kotsiantis SB. Decision trees: A recent overview. *Artif Intell Rev.* 2011;39:261-283.
doi: 10.1007/s10462-011-9272-4
 44. Breiman L. Random forests. *Mach Learn.* 2001;45:5-32.
doi: 10.1023/A:1010950718922
 45. Geurts P, Ernst D, Wehenkel L. Extremely randomized trees. *Mach*

- Learn. 2006;63:3-42.
doi: 10.1007/s10994-006-6226-1
46. Johnson R, Zhang T. Learning nonlinear functions using regularized greedy forest. *IEEE Trans Pattern Anal Mach Intell.* 2014;36:942-954.
doi: 10.1109/TPAMI.2013.159
47. LeCun Y, Bengio Y, Hinton G. Deep learning. *Nature.* 2015;521:436-444.
doi: 10.1038/nature14539
48. Reddy R, Kumar UMA. Classification of user's review using modified logistic regression technique. *Int J Syst Assur Eng Manag.* 2022;15:279-286.
doi: 10.1007/s13198-022-01711-4
49. Hearst MA. Support vector machines. *IEEE Intell Syst Their Appl.* 1998;13:18-21.
doi: 10.1109/5254.708428
50. Tharwat A, Gaber T, Ibrahim A, Hassanien AE. Linear discriminant analysis: A detailed tutorial. *AI Commun.* 2017;30:169-190.
doi: 10.3233/AIC-170729
51. Ghosh A, SahaRay R, Chakrabarty S, Bhadra S. Robust generalised quadratic discriminant analysis. *Pattern Recognit.* 2021;117:107981.
doi: 10.1016/j.patcog.2021.107981
52. Fei W, Changshui Z. Label propagation through linear neighborhoods. *IEEE Trans Knowl Data Eng.* 2008;20:55-67.
doi: 10.1109/TKDE.2007.190672
53. Csató L, Fokoué E, Opper M, Schottky B, Winther O. Efficient Approaches to Gaussian Process Classification. In: *Advances in Neural Information Processing Systems 12.* Vol. 12. 2000. p. 251-257.
54. Arpit D, Wu S, Natarajan P, Prasad R, Natarajan P. Ridge Regression based Classifiers for Large Scale Class Imbalanced Datasets. In: *2013 IEEE Workshop on Applications of Computer Vision (WACV).* Clearwater Beach, FL, USA: IEEE; 2013. p. 267-274.
doi: 10.1109/WACV.2013.6475028
55. Anand MV, KiranBala B, Srividhya SR, Kavitha C, Younus M, Rahman MH. Gaussian naïve bayes algorithm: A reliable technique involved in the assortment of the segregation in cancer. *Mob Inform Syst.* 2022;2022:1-7.
doi: 10.1155/2022/2436946
56. Sayfullina L, Eirola E, Komashinsky D, et al. Efficient Detection of Zero-day Android Malware Using Normalized Bernoulli Naive Bayes. In: *2015 IEEE Trustcom/BigDataSE/ISPA.* Helsinki, Finland: IEEE; 2015. p. 198-205.
doi: 10.1109/Trustcom.2015.375
57. Crammer K, Dekel O, Keshet J, Shalev-Shwartz S, Singer Y. Online passive-aggressive algorithms. *J Mach Learn Res.* 2006;7:551-585.

Received: December 19, 2024

Revised: March 25, 2025

Accepted: April 3, 2025

Available online: May 8, 2025